

# MATHEMATICAL MODELING OF FINES MIGRATION AND CLOGGING IN POROUS MEDIA

A Thesis  
Presented to  
The Academic Faculty

by

Guido Kampel

In Partial Fulfillment  
of the Requirements for the Degree  
Doctor of Philosophy in the  
School of Mathematics

Georgia Institute of Technology  
December 2007

# MATHEMATICAL MODELING OF FINES MIGRATION AND CLOGGING IN POROUS MEDIA

Approved by:

Professor Guillermo H. Goldsztein,  
Advisor  
School of Mathematics  
*Georgia Institute of Technology*

Professor Luca Dieci  
School of Mathematics  
*Georgia Institute of Technology*

Professor John McCuan  
School of Mathematics  
*Georgia Institute of Technology*

Professor Juan C. Santamarina  
School of Civil and Environmental  
Engineering  
*Georgia Institute of Technology*

Professor Haomin Zhou  
School of Mathematics  
*Georgia Institute of Technology*

Date Approved: July 30, 2007

## ACKNOWLEDGEMENTS

I would like to thank the members of my thesis committee for their time and dedication. I would like to thank my advisor, Professor G. Goldsztein, for his guidance throughout this process. Special thanks for Professor J. Santamarina, for introducing me to the topic of clogging in porous media, and for many valuable talks describing the physics of such processes.

Finally, I would like to thank my friends and family for their support.

# TABLE OF CONTENTS

ACKNOWLEDGEMENTS		iii
LIST OF TABLES		vii
LIST OF FIGURES		viii
SUMMARY		xi
I	INTRODUCTION	1
	1.1 Filters. The number of channels that can clog in a network	1
	1.2 Plugging of porous media near wells	3
	1.3 The effect of the micro-geometry on the performance of filters	6
II	FILTERS. THE NUMBER OF CHANNELS THAT CAN CLOG IN A NETWORK	8
	2.1 The model	9
	2.2 Review of concepts in graph theory	10
	2.3 Upper bound on the number of clogged channels	12
	2.3.1 Microstructure of the filters	12
	2.3.2 Clogged edges	13
	2.3.3 Mass conservation	14
	2.3.4 $C^*$ , a multigraph associated with the clogged edges	16
	2.3.5 Bounding the number of clogged edges	18
	2.4 Optimality of the bound	20
	2.4.1 Left most percolating paths	21
	2.4.2 First edge of a feasible sequence of edges	22
	2.4.3 Feasible sequence of edges of maximal length	25
	2.5 The bound in terms of the average degree of $G$ for large filters	28
	2.6 A subclass of filters and examples	29
	2.6.1 Subclass of filters. The geometries	30
	2.6.2 Subclass of filters. The width of the channels	31

2.6.3	The bound realizes for filters of class $\mathcal{A}$ . . . . .	32
2.6.4	Building filters of class $\mathcal{A}$ from thin filters . . . . .	33
2.6.5	Further comments on filters of class $\mathcal{A}$ . . . . .	35
III	PLUGGING OF POROUS MEDIA NEAR WELLS . . . . .	36
3.1	Macroscopic fines velocity as function of the macroscopic fluid velocity	37
3.1.1	Review. Hydrodynamic force on a spherical particle immerse in a fluid . . . . .	37
3.1.2	Average velocity of a particle flowing through a straight chan- nel when the particle is initially at rest at one end of the channel	38
3.1.3	Tortuosity of flow paths in porous media . . . . .	39
3.1.4	Relationship between the microscopic speed, the average ve- locity and the tortuosity . . . . .	40
3.1.5	Macroscopic fines velocity as function of the macroscopic fluid velocity . . . . .	41
3.1.6	Behavior of the macroscopic fines velocity vs. macroscopic fluid velocity curve . . . . .	41
3.2	Evolution equation for the concentration of fines and clogging criteria	42
3.2.1	Porosity . . . . .	42
3.2.2	Volume fraction of fines and volume fraction of fluid . . . . .	43
3.2.3	Fluid flow . . . . .	43
3.2.4	Macroscopic fines velocity as function of $r$ . . . . .	44
3.2.5	Transport of fines . . . . .	45
3.3	Fines accumulate as they are convected toward the inner boundary	46
3.4	Criterion for clogging . . . . .	47
3.5	Homogeneous initial conditions . . . . .	47
3.5.1	The concentration of fines is a decreasing function of $r$ . . . . .	47
3.5.2	Clogging may only occur at the inner boundary . . . . .	48
3.5.3	Determining if clogging does occur . . . . .	48
3.5.4	The parameter regime where the medium plugs . . . . .	50
3.5.5	Avoiding clogging . . . . .	51

3.5.6	Clogging time when clogging does occur . . . . .	52
3.5.7	Volume of fluid extracted before the medium plugs . . . . .	53
3.6	Conclusions . . . . .	55
IV	THE EFFECT OF THE MICRO-GEOMETRY ON THE PERFORMANCE OF FILTERS . . . . .	56
4.1	Mathematical model . . . . .	57
4.1.1	Fluid flow in channels . . . . .	57
4.1.2	Filter geometry . . . . .	57
4.1.3	Fluid flow in networks . . . . .	58
4.1.4	Particle transport within the filter . . . . .	60
4.1.5	Channels and particles size . . . . .	61
4.2	Probability that a particle is trapped in a clean filter . . . . .	61
4.2.1	One-dimensional filter . . . . .	62
4.2.2	Two dimensional filters . . . . .	65
4.3	Numerical simulations of filters . . . . .	71
APPENDIX A	. . . . .	76

## LIST OF TABLES

1	Asymptotic value in the $n$ large limit of the probability $P$ that a particle of diameter with distribution $d$ crosses through a one-dimensional tube of $n$ channels of width with distribution $\delta$ without being trapped. The probabilities in the last column are calculated according to equation (75).	65
2	Numerically computed values of the probability $P$ that a particle flows through the clean filter without being trapped. Figure 24 shows the associated linear fit for the logarithms. . . . .	66
3	Numerically computed values of the probability $P$ that a particle flows through the clean filter without being trapped. Note that tables (a) and (b) have equal one-dimensional fit. Figure 25 shows the associated linear fits for the logarithms. . . . .	67
4	Numerically computed values of the probability $P$ that a particle flows through the clean filter without being trapped. Note that tables (a) and (b) have equal one-dimensional fit. Figure 26 shows the associated linear fits for the logarithms. . . . .	68
5	Numerically computed values of the probability $P$ that a particle flows through the clean filter without being trapped. Figure 27 shows the associated linear fit for the logarithms. . . . .	69
6	Results from numerical simulations. We compare the cleaned fluid (per column of the network), the percentage of clogged channels and the average life flow rate (per column of the network) for different filters.	72

# LIST OF FIGURES

1	Illustration of Santamarina and Valdes experiment [62]. The gray area is the two-dimensional porous medium. The arrows in the left figure indicate the average direction of the flow. The middle figure shows a microscopic look at the material. The dark region is the solid matrix. Suspension can only flow through the white region. The right figure shows a plugged medium. The region clogged is in dark. . . . .	5
2	Network of channels. The solid material is in gray. The white spaces are the channels. The arrows indicate the direction of the flow in the channels next to the top and the bottom boundary. . . . .	9
3	Multigraph $G$ . The black small circles are the nodes of the multigraph $G$ and the solid lines its edges. . . . .	13
4	Example of a multigraph $G$ . The edges of $G$ are the thin and thick solid lines. The dashed lines are not part of $G$ . $F_i$ ( $1 \leq i \leq 10$ ) are the connected components of $\{y_b < y < y_t\} - G$ . The edges in thick solid lines are not contained in any percolating path. The edges in thin solid lines are contained in percolating paths. There can be flow only through the thin edges. . . . .	16
5	The clogged edges are thick solid lines. The open edged in thin solid lines. The thick dashed lines are the edges in $C^*$ . The white circles are the nodes of $C^*$ . . . . .	18
6	The four different possibilities of observation 2.4.1. We do not show all the multigraph $G$ , only $e$ , $\bar{Q}$ and $P$ . The edge $e$ is the segment between the solid small circles. $P$ is the thin solid vertical line, $\bar{Q}$ the thick solid line, and $R$ the union of $\bar{Q}$ and the dashed lines. . . . .	21
7	Multigraph $G$ . $\partial F \cap \{y = y_b\}$ is the edge in dashed line and the white nodes, which is a disconnected set. The thick solid line is $\bar{Q}$ . The edges in $\bar{Q}$ are not included in any percolating path of $G$ . . . . .	23
8	Multigraph $G$ . The edges of the path $S$ are in thick lines. Example of a sequence $F_0, F_1, F_2 = F$ constructed as in observation 2.4.5. . . . .	24
9	Four different possibilities of $F$ from observation 2.4.6 and theorem 2. The solid line is the percolating path $S$ of observation 2.4.6. The left vertical line is $P$ . $P \cap S$ is in solid line and the section of $P$ that does not intersect $S$ is in dashed line. The dashed horizontal lines are the sections of the top and bottom boundary that are to the left of $S$ . . .	26

10	Four different possibilities of the percolating path $Q$ , in thick solid lines, from observation 2.4.6. The edge $e$ is between the solid small circles. The left vertical line is $P$ . . . . .	26
11	Multigraphs with geometries of class $\mathcal{A}$ . The percolating paths $P_i$ are in solid lines. The crossing paths $H_{i,j}$ are in dashed lines. . . . .	30
12	Multigraphs of figure 11. The thick edges are in solid lines. Thin edges in dashed lines. . . . .	32
13	Building a filter of class $\mathcal{A}$ . In the top figure we start with a thin filter with thin channels. In the middle figure we fold the thin filter. The bottom figure shows the resulting filter after folding and compressing. The thick edges are in solid thick lines. The thin edges are in dashed lines. . . . .	34
14	Channel of length $L$ filled with an incompressible fluid. The arrow indicate the direction of the flow. The black circle is a particle that will move toward the right end due to hydrodynamic forces. . . . .	38
15	The small segments form a typical path traveled by an element of fluid in a porous medium. . . . .	40
16	Plot of $v/\alpha$ vs. $u/\alpha$ . Both plots correspond to the same curve. They are just in different scales. . . . .	42
17	Plot of $\alpha r/A$ vs. $u/\alpha$ . Both plots correspond to the same curve. They are just in different scales. . . . .	45
18	Plot $r/R_\ell$ vs. $z$ for four fixed values of $t$ : $t = 0$ , $t = R_\ell/\alpha$ , $t = 5R_\ell/\alpha$ and $t = 100R_\ell/\alpha$ . $z$ increases with $t$ . . . . .	47
19	Regions in the parameter plane $z_*/z_0$ vs. $A/(\alpha R_\ell)$ where clogging does and does not occur. Both plots correspond to the same regions. They are just in different scales. . . . .	51
20	$A/(\alpha R_\ell)$ vs. $\alpha t_c/R\ell$ where $z_*/z_0 = 2$ . . . . .	53
21	$A/(\alpha R_\ell)$ vs. $V_f/R_\ell^2$ where $z_*/z_0 = 2$ . . . . .	54
22	Velocity profile of a Poiseuille flow within a straight channel (indicated by arrows). . . . .	57
23	Example of a network of one of our filters and the corresponding graph. . . . .	58
24	Linear fits for values from table 2 in $\log_2 - \log_2$ scale. The purple dots are the numerically computed $P$ probabilities. The red line is the linear fit for these points. The green dots are the one-dimensional asymptotics, and the blue line its linear fit. . . . .	67

25 Linear fits for values from tables 3 in  $\log_2 - \log_2$  scale. The purple dots are the numerically computed  $P$  probabilities of table 3(a). The red line is the linear fit for these points. The pink dots and black line corresponds to 3(b). The green dots are the one-dimensional asymptotics, and the blue line its linear fit. Recall that one-dimensional asymptotics is equal for both networks. . . . . 68

26 Linear fits for values from tables 4 in  $\log_2 - \log_2$  scale. The purple dots are the numerically computed  $P$  probabilities of table 4(a). The red line is the linear fit for these points. The pink dots and black line corresponds to 4(b). The green dots are the one-dimensional asymptotics, and the blue line its linear fit. Recall that one-dimensional asymptotics is equal for both networks. . . . . 69

27 Linear fits for values from table 5 in  $\log_2 - \log_2$  scale. The purple dots are the numerically computed  $P$  probabilities. The red line is the linear fit for these points. The green dots are the one-dimensional asymptotics, and the blue line its linear fit. . . . . 70

28 A section of a square filter of class  $\mathcal{A}$  after clogging. The clogged channels are not shown, and a trapped particle is shown instead. The thick channels are in red. All the thin channels are clogged. . . . . 73

29 A section of a filter with  $\delta \sim U(0.18, 0.5)$  after clogging. The clogged channels are not shown, and a trapped particle is shown instead. The color intensity of the open channels indicates width, varying from blue, that corresponds to 0.5 to light blue, that corresponds to 0.18. Note that most particles are trapped close to the bottom boundary. . . . . 74

30 A section of a filter with discrete probability distribution  $P(\delta = 0.5) = 0.55$  after clogging. The thick channels are in red, the thin open channels in blue, and there is a particle whenever a channel is clogged. We note that the percolating paths of thick channels are few. . . . . 75

## SUMMARY

A porous medium is a material that contains regions filled with fluid embedded in a solid matrix. These fluid filled regions are called pores or voids. Suspensions are fluids with small particles called fines. As a suspension flows through a porous material, some fines are trapped within the material while others that were trapped may be released.

Filters are an example of porous media. We model filters as networks of channels. As a suspension flows across the filter, particles clog channels. We assume that there is no flow through clogged channels. In the first part of this thesis, we compute a sharp upper bound on the number of channels that can clog before fluid can no longer flow through the filter.

Soil mass is another example of porous media. Fluid in porous media flows through tortuous paths. This tortuosity and inertial effects cause fines to collide with pore walls. After each collision, a particle loses momentum and needs to be accelerated again by hydrodynamic forces. As a result, the average velocity of fines is smaller than that of the fluid. This retardation of the fines with respect to the fluid may lead to an increase of the concentration of fines in certain regions which may eventually result in the plugging of the porous medium. This effect is of importance in flows near wells where the flow has circular symmetry and thus, it is not macroscopically homogeneous. In the second part of this thesis we develop and analyze a mathematical model to study the physical effect described above.

In the third and last part of this thesis we study particle migration and clogging as suspension flows through filters by means of numerical simulations and elementary analysis. We model filters as networks of channels. Each channel is either open or

clogged. There is no flow through clogged channels. Each particle and each channel is assigned a width. Particles flow with the fluid while inside a wider channel. When reaching an intersection of channels, a particle flows into a new channel. If this new channel is thinner than the particle, the particle is trapped and the channel clogged. We explore the effect that network geometry, probability distribution of the width of the channels and probability distribution of the diameter of the particles have on the performance of filters.

# CHAPTER I

## INTRODUCTION

A porous medium is a material that contains spaces filled with fluid embedded in a solid matrix. These fluid filled spaces are called pores or voids. A porous material is said to be permeable if fluid can flow from one region of the material to another through its voids. Suspensions are fluids with small particles. According to their size and properties, these particles are called fines or colloids. As suspension flows through a permeable porous material, some fines are trapped within the material while others that were trapped may be released due to hydrodynamic or other forces.

### ***1.1 Filters. The number of channels that can clog in a network***

Filters are examples of porous materials. In fact, our study in chapter 2 is motivated by filters whose function is to clean fluids by capturing most particles bigger than a certain size.

The removal of particles from fluids is of importance in a wide range of industrial and technological applications such as waste water treatment [27], refining of liquid aluminum, catalysis, liquid chromatography, oil recovery [8, 59] among many others. Our studies are motivated by the filters used in the process known as deep bed filtration. As suspension flows through a filter composed of granular or fibrous materials, fines or colloidal particles penetrate the filter and deposit at various depths [60]. As a result, the fluid is cleaner after it exits the filter.

Theoretical models to study transport in porous media can be classified in either macro-scale [9, 22, 35, 37, 38, 44, 60] or pore-scale models [13, 31, 46]. Within the later group, the class of network models, in which the pore space is modeled as a network

of channels, is very popular. Network models provide flexibility to model different geometries of pore space while keeping the computational cost not very high. Our work in chapter 2 belongs to this class of models.

Network models to study flow in porous media were introduced by Fatt in 1956 [15, 16, 17]. Donaldson, in 1977 [12], was the first one to use networks to study particle transport within porous media. The clogging of particles has been studied in networks with different geometries including bundle of parallel tubes [12], square networks [21, 23, 33], triangular networks [7, 43], cubic networks [6, 24, 56], bubble models [10, 32], and the so called three-dimensional physically representative networks [5, 58].

Consider a filter that is a network of channels. As suspension flows through the filter, particles clog channels. Assume suspension can not flow through clogged channels. Note that there can only be flow through channels that are part of a percolating path of un-clogged channels, i.e. a path of channels that are un-clogged connecting one side of the filter with the opposite side. As channels clog, some percolating paths of not clogged channels are broken. Thus, suspension stops flowing not only through the clogged channels, but also through other channels, i.e. those that are no longer part of a percolating path of not clogged channels. Thus, the filter will stop being permeable when not all, but only a number of its channels clog. In chapter 2 we find an upper bound of this number. Our upper bound is a function of the geometry of the network. In particular, we are able to identify the filter's geometries for which the largest fraction of channels may be clogged before the filter ceases to be permeable, suggesting that filters with these geometries may have longer lives than others.

Our work is novel. Most of the work that can be found in the literature consists of simulations of the suspension dynamics within the medium. Our work is an analysis that is independent of the dynamics, it depends only on the topology of the network. On the other hand, our work has connections, but also key differences, with the theory

of bond percolation [19, 45]. In particular, we are able to use graph theory techniques that are also used in percolation theory. However, in percolation theory, channels or edges are removed randomly and independently of each other. For us, channels clog, but not randomly nor independently of each other: It is important the order in which they clog.

## ***1.2 Plugging of porous media near wells***

Soil mass is an other example of porous media. The particles that hold the soil together form the solid matrix that in this case of soils is known as the load carrying skeleton. Fines are small particles that do not form part of this skeleton and may be carried by the flow and be trapped at other locations or exit the porous medium. The sites that trap fines are usually pore constrictions or pore throats, i.e. the thinner regions of the voids. For example, if several migrating particles reach a small pore throat simultaneously, the particles may bridge across and clog the pore throat. The clogging of pore throats decreases the overall flow in the medium which may eventually become plugged, i.e. the medium is no longer permeable. The physics that determine the dynamics of fines and the plugging of porous media is complex. More detailed discussions can be found in [3, 4, 20, 26, 31, 39, 40, 41, 48, 50, 53, 52, 62].

In chapter 3, as explained next, we study only a partial set of effects that may lead to the plugging of porous media. Fluid in porous media flows through tortuous paths, i.e. paths that are not straight. This tortuosity and inertial effects cause fines to collide with pore walls. After each collision, a particle losses momentum and needs to be accelerated again by the fluid through hydrodynamic forces. As a result, the average velocity of fines is smaller than that of the fluid.

To simplify the discussion that will follow, we now introduce some notation. We will denote by  $\mathbf{v}$  what we call the *macroscopic* fluid velocity, i.e.  $\mathbf{v}$  is the average of the fluid velocity in regions much larger than the pores but much smaller than

the material. Note that, in principle,  $\mathbf{v}$  is a function of the spatial position  $\mathbf{x}$  and time  $t$ , i.e.  $\mathbf{v} = \mathbf{v}(\mathbf{x}, t)$ . We denote by  $\mathbf{u}$  the *macroscopic* fines velocity, i.e.  $\mathbf{u}$  is the average of the velocities of the fines in regions much larger than the pores but much smaller than the material. Note that, according with the discussion of the above paragraph,  $\|\mathbf{u}(\mathbf{x}, t)\| \leq \|\mathbf{v}(\mathbf{x}, t)\|$ , where  $\|\mathbf{u}(\mathbf{x}, t)\|$  denotes the euclidean norm of the vector  $\mathbf{u}(\mathbf{x}, t)$ .

If the macroscopic fluid velocity is spatially homogeneous, i.e.  $\mathbf{v}$  is independent of  $\mathbf{x}$ , the macroscopic fines velocity  $\mathbf{u}$  will also be independent of  $\mathbf{x}$ . Thus, the location of the maximum concentration of fines in space will travel at velocity  $\mathbf{u}$  but the concentration value will not change. On the other hand, if  $\mathbf{v}$  is not independent of  $\mathbf{x}$ ,  $\mathbf{u}$  will not be independent of  $\mathbf{x}$  either. As a consequence, both the location and the value of the maximum concentration of fines in space will change with time. In particular, the concentration of fines may exceed some critical value that leads to the clogging of pore throats and eventually the plugging of the medium. Motivated by the clogging that is sometimes observed in petroleum and water wells, we will consider two-dimensional macroscopic flows with circular symmetry. Clearly, the macroscopic fluid velocity is not spatially homogeneous in this case, it decays with the distance to the well.

Our studies are also motivated by a series of laboratory experiments conducted by Santamarina and Valdes [62]. In fact, they propose that the physical effects we model in this thesis are important factors in the plugging of porous media around wells. They use a circular sheet of emery sandpaper as a two-dimensional porous medium. A heavy plane plate is placed on top of the rough side of the sandpaper that rests over a foam layer on a plane surface. The purpose of the foam is to maximize the contact between the plate and the sandpaper and to distribute this contact evenly. The center of the sandpaper has a circular orifice. The outer edge of the porous medium is placed in contact with a suspension reservoir (fluid with fines). An imposed pressure at the

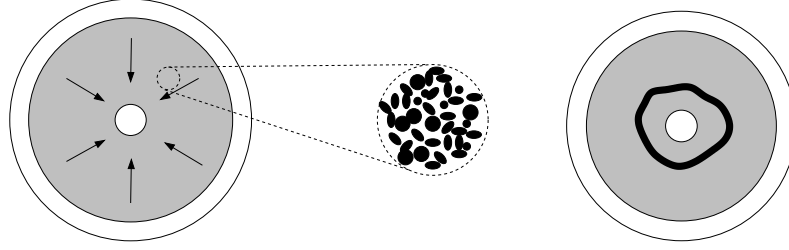


**Figure 1:** Illustration of Santamarina and Valdes experiment [62]. The gray area is the two-dimensional porous medium. The arrows in the left figure indicate the average direction of the flow. The middle figure shows a microscopic look at the material. The dark region is the solid matrix. Suspension can only flow through the white region. The right figure shows a plugged medium. The region clogged is in dark.

outer edge, higher than the pressure at the orifice, creates a suspension flow in the space enclosed between the sandpaper and the plate. The suspension flows from the outer edge toward the orifice in the center of the sandpaper where it exits the device (see figure 1).

Both clogging and not clogging were observed. Whether clogging occurs or not, depends on the parameter regime of the experiment (i.e. particle size and concentration, applied pressure, etc). Whenever the medium clogged, they always observed that the pore throats clogged were not evenly distributed throughout the medium. Instead, they were concentrated at a certain distance from the orifice, forming an easily observable ring of trapped particles (see figure 1).

Our approach can be considered to be a multi-scale one. As a first step we develop a pore-scale mathematical model that allows us to obtain the macroscopic fines velocity  $\mathbf{u}$  as a function of the macroscopic fluid velocity  $\mathbf{v}$ . This pore-scale model results from assuming that any given particle follows a tortuous path that consist of a sequence of straight channels of length  $L$  and that, each time that a particle reaches the end of a channel, it collides with the pore wall and losses all its momentum. Thus, each time the particle enters a new channel, it starts traveling through the channel with an initial velocity equal to zero and it accelerates due to

hydrodynamic forces.

As a second step we introduce a macro-scale mathematical model that describes the time evolution of concentration of fines. This model results from the fact that the concentration of fines is convected with velocity  $\mathbf{u}$ . We also propose that regions of the medium plug if and when the concentrations of fines in those regions exceed a certain critical value. The model in this second step belongs to the class of macroscopic models, i.e. models that keep track of the concentration of particles at the macroscopic-scale, i.e. in regions in space much smaller than the medium size but much larger than particle and pore sizes.

While there exists a large number of macroscopic mathematical models of migration of fines and clogging, some of the most popular ones include [64, 42, 36, 22, 28, 20, 55, 46, 47, 37, 1], our model is truly novel. Our modeling efforts focus on physical effects that, to the best of our knowledge, have not been modeled before. Our goal is to develop a simple model that captures the main features of the physical effects previously described that, in our opinion, play a fundamental role in the plugging of porous media near wells. We believe we accomplish our goal in the present work and this work will serve as a step toward more comprehensive modeling of plugging of porous media and it will also suggest experiments to test hypothesis to eventually provide a better understanding of the physics involved in this complex but technologically important process.

### ***1.3 The effect of the micro-geometry on the performance of filters***

In chapter 4 we study particle migration and clogging as suspension flows through filters by means of numerical simulations and elementary analysis. We model filters as networks of channels. Each channel is either open or clogged. There is no flow through clogged channels. Each particle and each channel is assigned a width. Particles flow with the fluid while inside a wider channel. When reaching an intersection of channels,

a particle flows into a new channel. If this new channel is thinner than the particle, the particle is trapped and the channel clogged.

The geometries of the networks we study in this chapter are regular: one-dimensional network and two-dimensional square and hexagonal networks. We study the case when the widths of the channels and of the particles are independent random variables. We select a probability distribution for the width of the channels and a second one for the width of the particles. Among other questions, in this chapter we seek to answer the following questions in terms of the geometry of the network, the probability distribution of the width of the channels and the probability distribution of the width of the particles:

1. What is the proportion of particles that are trapped?
2. What is the proportion of channels clogged when the filter ceases to be effective?
3. How does the filter permeability decreases during its life time?

We also study some deterministic filters, i.e. the width of the channels and particles are not random, that are optimal in some sense.

There exists a large list of works emphasizing empirical considerations for improving filter performances [57, 25, 29, 61]. While needed, the mathematical modeling of the general behavior of filters is still limited. Some important models are [54, 10, 51, 30, 34, 63, 18].

Our work is novel. We use asymptotic techniques that allow us to draw general conclusions. On the other hand, in chapter 2 we suggest a filter design, which is subject to particular comparisons in the simulations of chapter 4.

## CHAPTER II

### FILTERS. THE NUMBER OF CHANNELS THAT CAN CLOG IN A NETWORK

Consider a filter that is a network of channels. As suspension flows through the filter, particles clog channels. Assume suspension can not flow through clogged channels. Note that there can only be flow through channels that are part of a percolating path of not clogged channels, i.e. a path of channels that are not clogged connecting one side of the filter with the opposite side. As channels clog, some percolating paths of un-clogged channels are broken. Thus, suspension stops flowing not only through the clogged channels, but also through other channels, i.e. those that are no longer part of a percolating path of un-clogged channels. Thus, the filter will stop being permeable after not all, but only some of its channels clog. As previewed in the introduction, in this chapter we find an upper bound of the number of channels that clog. Our upper bound is a function of the geometry of the network. In particular, we are able to identify the filter's geometries for which the largest fraction of channels may be clogged before the filter ceases to be permeable, suggesting that filters with these geometries may have longer lives than others.

This chapter is organized as follows. In section 2.1, we describe the filters as networks. In section 2.2, we review the basics of graph theory needed in the rest of this chapter. In section 2.3, we obtain our upper bound. In section 2.4, we show that our upper bound is sharp. In section 2.5, we consider large filters and obtain an alternative description of our bound in terms of the average degree of the network. In section 2.6, we consider a special class of filters for which our bound is realized. In section 2.6, we also consider some examples and obtain some conclusions.

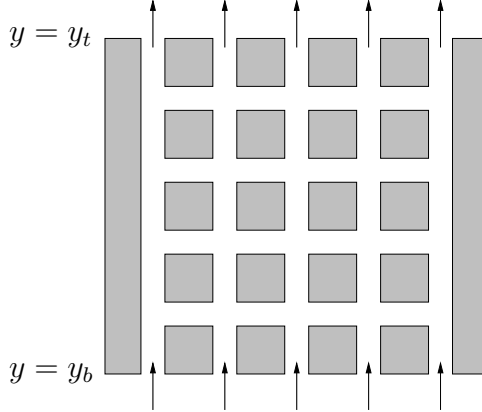


**Figure 2:** Network of channels. The solid material is in gray. The white spaces are the channels. The arrows indicate the direction of the flow in the channels next to the top and the bottom boundary.

## 2.1 *The model*

We model filters as two-dimensional networks of channels as we illustrate in figure 2. The voids are the interior of the channels. Our filters have a bottom boundary at  $y = y_b$  and a top boundary at  $y = y_t$ .

In our model, channels are either open or clogged. Suspension can only flow through open channels. There is no flow through clogged channels. Within an open channel, suspension flows from the end with higher pressure to the opposite end. If both ends are at the same pressure, there is no flow within the channel.

We assume that suspension can only flow into the filter through the bottom boundary, and can flow out of the filter only through the top boundary. Both fluid and particles are incompressible and thus, volume of suspension enters the filter through the bottom boundary at the same rate it exits the filter through the top boundary.

We assume that the bottom boundary is held at constant pressure  $p = p_b$  and the top boundary at  $p = p_t$ , where  $p_b > p_t$ . Note that the filter is permeable if and only if there is a path of open channels connecting the bottom boundary with the top boundary. Due to the difference in pressure between the top and bottom boundaries, there is flow through the filter if and only if it is permeable.

We assume that initially all the channels are open. As suspension flows through the filter, particles are trapped causing channels to clog, i.e. channels change from open to clogged. Eventually, the filter is no longer permeable. Note that an open channel can only clog if there is flow through it. For any given filter, we will find an upper bound on the number of channels that may clog under the assumption that different channels do not clog at the same time.

**Assumptions 2.1.1.** *For future reference, we list here the key assumptions of our model.*

1. *Channels are either open or clogged.*
2. *There is no flow through clogged channels.*
3. *Suspension can only flow into the filter through the bottom boundary and out of the filter through the top boundary.*
4. *Fluid and particles are incompressible.*
5. *Initially all the channels are open.*
6. *An open channel may clog if there is flow through it.*
7. *An open channel does not clog if there is no flow through it.*
8. *Different channels do not clog at the same time.*

## **2.2 Review of concepts in graph theory**

In this section we review concepts of graph theory that we need in the rest of the chapter. More details on graph theory can be found in [11].

A *graph*  $G$  consists of a non-empty set of elements, called *vertices* or *nodes*, and a list of unordered pairs of these elements, called *edges*. It is convenient and a common practice to draw graphs in the plane. Each node is a different point and each edge a

line joining its two nodes without intersecting any other node. If  $e$  is an edge joining the two nodes  $a$  and  $b$ , we say that  $a$  and  $b$  are the end points of  $e$  and that  $e$  connects  $a$  and  $b$ . For convenience we take  $e$  (the drawing of  $e$  really) to be a closed set, i.e.  $e$  includes its end points. If  $a = b$ , i.e. the end points of an edge  $e$  are the same, we say that  $e$  is a loop. In a graph, two different edges do not have the same pair of end points. We have a *multigraph* when this restriction is removed, i.e. in a multigraph, two different edges can have the same end points.

We say that two nodes  $a$  and  $b$  are connected if there exist a sequence of nodes  $n_0, n_1, \dots, n_k$  such that  $a = n_0$ ,  $b = n_k$  and for each  $1 \leq i \leq k$  there exists an edge  $e_i$  that connects  $n_{i-1}$  and  $n_i$ . In this case, the alternating sequence of nodes and edges  $n_0, e_1, n_1, e_2, n_2, \dots, e_k, n_k$  forms a *walk* between  $a$  and  $b$  or simply a *walk*. We say that  $a = n_0$  and  $b = n_k$  are the end points of the walk. If  $n_i \neq n_j$  for all  $i \neq j$ , we say that the walk is a *path*. If  $n_0 = n_k$  and  $n_i \neq n_j$  for  $i < j$  except when  $(i, j) = (0, k)$ , we say that the walk is a *cycle*. We will identify each walk with the curve in the plane formed by its edges.

Let  $G$  be a multigraph.  $S$  is a *submultigraph* of  $G$  if  $S$  is a multigraph and  $S$  is included in  $G$ , i.e. every node of  $S$  is also a node of  $G$  and every edge of  $S$  is also an edge of  $G$ .

A multigraph is *connected* if there is a walk between any pair of nodes, and *disconnected* otherwise. Every disconnected multigraph is the union of connected submultigraphs where each node of the multigraph belongs exactly to one submultigraph. Each of these submultigraphs is called a *connected component* of the multigraph.

A multigraph is *planar* if it can be drawn in the plane in such a way that any two different edges may only intersect at one or two of their end points. Any such drawing is a *plane drawing* of the multigraph. In this chapter we will only need to consider planar multigraphs. We identify each planar multigraph with one of its plane drawings. In the rest of this chapter, any multigraph that we mention or consider is

a planar multigraph.

A multigraph divides the plane into regions called *faces*. In other words, the faces are the connected components of what is left from the plane once we remove the multigraph. Note that the faces are open sets. Any finite multigraph has an unbounded face surrounding it, called the *infinity face*.

The boundary of a bounded face contains a cycle. Thus, a connected multigraph with no cycles has only one face, the infinity face.

Let  $G$  be a multigraph. We denote by  $n_G$  its number of nodes, by  $e_G$  its number of edges, by  $f_G$  its number of faces and by  $\ell_G$  its number of connected components. The well known *Euler formula* states that

$$n_G + f_G = e_G + \ell_G + 1. \quad (1)$$

The degree of a node  $n$ , that we denote by  $d_n$ , is the number of edges that have  $n$  as end point, where the loops are counted twice. The average degree of a multigraph  $G$ , that we denote by  $d_G$ , is defined as the average of the degrees of the nodes of  $G$ ,  $d_G = n_G^{-1} \sum_{n \text{ node of } G} d_n$ , where  $n_G$  is the number of nodes of  $G$ . Note that

$$d_G = 2 \frac{e_G}{n_G}, \quad (2)$$

where  $e_G$  is the number of edges of  $G$ . An example of a multigraph, that is actually a graph, is shown in figure 3.

## ***2.3 Upper bound on the number of clogged channels***

### **2.3.1 Microstructure of the filters**

To each filter we associate a multigraph in a natural way. The edges are the channels and the nodes the end points of the edges.

Recall that the bottom and top boundaries of the filter are located at  $y = y_b$  and  $y = y_t$  respectively. Thus, the multigraph is included in  $y_b \leq y \leq y_t$ . Note that there are nodes in the bottom and top boundaries. For convenience, we also include

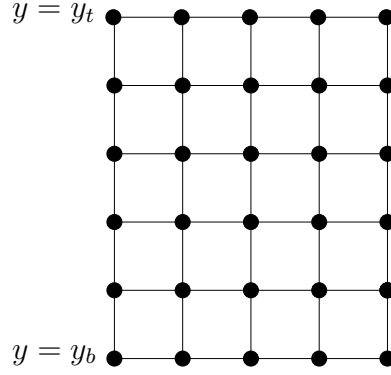


**Figure 3:** Multigraph  $G$ . The black small circles are the nodes of the multigraph  $G$  and the solid lines its edges.

edges in  $y = y_b$  connecting the nodes in the bottom boundary. In other words, there is a path of edges in  $y = y_b$  connecting the left most node in the bottom boundary with the right most node in that boundary. Analogously, we include edges in  $y = y_t$  so that there is a path of edges in  $y = y_t$  connecting the left most node in the top boundary with the right most node in that boundary.

We consider filters with a finite number of channels, thus our multigraphs are finite multigraphs, i.e. they contain a finite number of nodes and edges. As an example, in figure 3 we show the multigraph  $G$  associated with the filter of figure 2.

**Definition 1.** *We say that a node is an exterior node if it is located at  $y = y_b$  or  $y = y_t$ . Otherwise, we say that the node is an interior node.*

*We also say that an edge is an exterior edge if it is included in  $\{y = y_b\} \cup \{y = y_t\}$ . Otherwise, we say that the edge is an interior edge.*

Note that, by construction, each exterior node is the end point of a least one interior edge.

### 2.3.2 Clogged edges

Suspension enters the network through exterior nodes at  $y = y_b$  and exits the network through exterior nodes at  $y = y_t$ .

We say that an edge is clogged if the corresponding channel is clogged. Note that the exterior edges were included for convenience, they do not correspond to any channel. Thus, we assume that there is no flow within them and that they never clog, i.e. they are always open.

As we said in section 2.1, we assume that initially all the edges were open and that, as suspension flowed through the filter, edges clogged but different edges did not clog simultaneously.

We study our filter at a fixed time. In other words, when we say that an edge is clogged, we mean that the edge is clogged at that fixed time. Analogously, when we say that an edge is open, we mean open at that fixed time.

### 2.3.3 Mass conservation

In this subsection we introduce a definition and an observation that we will need later in the chapter. This observation is a consequence of the law of mass conservation. Here, as in the rest of this section,  $G$  is a fixed multigraph that corresponds to one of our filters, such as the one in figure 3.

**Definition 2.** *Let  $\Omega$  be an open bounded set of  $\mathbb{R}^2$  such that  $\bar{\Omega}$ , the closure of  $\Omega$ , does not intersect any exterior edge of  $G$ , and  $\partial\Omega$ , the boundary of  $\Omega$ , does not contain any node of  $G$ . We define:*

$$E_{\Omega} = \{\text{edges in } G \text{ with exactly one end point in } \Omega\}, \quad (3)$$

$$E_{\Omega}^{\text{in}} = \{e \in E_{\Omega} : \text{suspension flows through } e \text{ into } \Omega\} \quad (4)$$

and

$$E_{\Omega}^{\text{out}} = \{e \in E_{\Omega} : \text{suspension flows through } e \text{ out of } \Omega\}. \quad (5)$$

Since there may be some edges without flow through them, the union of  $E_{\Omega}^{\text{in}}$  and  $E_{\Omega}^{\text{out}}$  need not be  $E_{\Omega}$ . In particular, clogged edges in  $E_{\Omega}$  are neither in  $E_{\Omega}^{\text{in}}$  nor  $E_{\Omega}^{\text{out}}$ .

Note that there may also be open edges  $E_\Omega$  without flow through them. Thus, there may be open edges in  $E_\Omega$  that are neither in  $E_\Omega^{\text{in}}$  nor  $E_\Omega^{\text{out}}$ . Note also that  $E_\Omega^{\text{in}}$  and  $E_\Omega^{\text{out}}$  are disjoint sets.

**Observation 2.3.1.** *Let  $\Omega$  be an open bounded set of  $\mathbb{R}^2$  such that  $\bar{\Omega}$  does not intersect any of the exterior edges of  $G$  and  $\partial\Omega$  does not contain any node of  $G$ . Then:*

1. *The rate at which suspension flows into  $\Omega$  through the edges in  $E_\Omega^{\text{in}}$  is equal to the rate at which suspension flows out of  $\Omega$  through the edges in  $E_\Omega^{\text{out}}$ .*
2. *Let  $e \in E_\Omega$ . If all the other edges in  $E_\Omega$  are clogged, then there is no flow through  $e$ .*
3. *If  $E_\Omega$  is not empty, then at least one of the edges in  $E_\Omega$  is not clogged.*

*Proof.* Suspension can only flow into the filter through its bottom boundary (i.e. the exterior nodes at  $y = y_b$ ) and out of the filter through its top boundary. This, together with the facts that  $\Omega$  does not contain any of the exterior nodes, the suspension is incompressible and there are neither mass sources nor mass sinks within the filter, imply point 1.

To prove point 2, let  $e$  be an edge in  $E_\Omega$  and assume that any edge in  $E_\Omega$  other than  $e$  is clogged. Thus, we have that  $e$  is the only element that can belong to either  $E_\Omega^{\text{in}}$  or  $E_\Omega^{\text{out}}$ . On the other hand, from point 1,  $E_\Omega^{\text{in}}$  is not empty if and only if  $E_\Omega^{\text{out}}$  is not empty and thus, since  $E_\Omega^{\text{in}}$  and  $E_\Omega^{\text{out}}$  are disjoint,  $E_\Omega^{\text{in}} \cup E_\Omega^{\text{out}}$  can not consist of a single element. We conclude that  $E_\Omega^{\text{in}} \cup E_\Omega^{\text{out}}$  is empty and thus, there is no flow through  $e$ , which proves point 2.

We prove point 3 by contradiction. Assume that all the edges in  $E_\Omega$  are clogged. Let  $e$  be the edge in  $E_\Omega$  that clogged last. Once the other edges were clogged, there was no more flow through  $e$  and thus,  $e$  could not have clogged because our model assumes an open edge does not clog if there is no flow through the edge.  $\square$

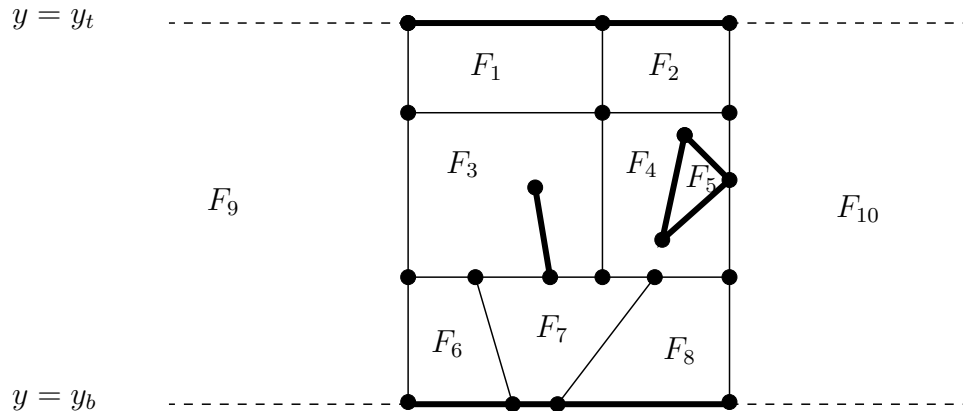


**Figure 4:** Example of a multigraph  $G$ . The edges of  $G$  are the thin and thick solid lines. The dashed lines are not part of  $G$ .  $F_i$  ( $1 \leq i \leq 10$ ) are the connected components of  $\{y_b < y < y_t\} - G$ . The edges in thick solid lines are not contained in any percolating path. The edges in thin solid lines are contained in percolating paths. There can be flow only through the thin edges.

### 2.3.4 $C^*$ , a multigraph associated with the clogged edges

In this subsection we construct a multigraph  $C^*$  that is associated with the set of clogged edges.

We first note that the bounded connected components of the set  $\{y_b < y < y_t\} - G$  are the bounded faces of  $G$ . In addition,  $\{y_b < y < y_t\} - G$  has two unbounded connected components, one to the left of  $G$  and the other to its right. An example is shown in figure 4, where the edges of  $G$  are the thin and thick solid lines. The dashed lines are not part of  $G$ .  $F_i$  ( $1 \leq i \leq 10$ ) are the connected components of  $\{y_b < y < y_t\} - G$ . While  $F_i$  for  $1 \leq i \leq 8$  are the bounded faces of  $G$ ,  $F_9$  and  $F_{10}$  are not faces of  $G$ .

Before proceeding with the construction of  $C^*$  we first need some preliminary definitions and observations.

**Definition 3.** We say that a path  $P = n_0, e_1, n_1, \dots, e_r, n_r$  in  $G$  is a percolating path if  $n_0$  is a bottom exterior node,  $n_r$  is a top exterior node and  $n_1, \dots, n_{r-1}$  are interior nodes.

**Observation 2.3.2.** *Let  $e$  be an edge in  $G$ . If there is no percolating path that contains  $e$ , then  $e$  never clogs.*

The claim of observation 2.3.2 is illustrated in figure 4. Let  $e$  be an edge of  $G$ . If there is no percolating path that contains  $e$ , then the pressure at the end points of  $e$  are equal which implies that there is no flow through  $e$  and thus,  $e$  can never clog.

Note that all percolating paths split the strip  $\{y_b \leq y \leq y_t\}$  in two connected components, one to the right of the path and the other to its left.

**Definition 4.** *Let  $P$  be a percolating path. We say that a set  $S$  is to the right of  $P$  if  $S$  is included in the closure of the right connected component of  $\{y_b \leq y \leq y_t\} - P$ . Analogously,  $S$  is to the left of  $P$  if  $S$  is included in the closure of the left connected component of  $\{y_b \leq y \leq y_t\} - P$ .*

**Observation 2.3.3.** *Let  $P$  be a percolating path and  $F$  a connected component of  $\{y_b < y < y_t\} - G$ . Then,  $F$  is either to the right of  $P$  or to the left of  $P$ .*

While obvious, the last observation leads to the next one that will be key in our construction of  $C^*$

**Observation 2.3.4.** *Let  $e$  be an edge in  $G$ . If there is a percolating path that contains  $e$ , then  $e$  is in the boundary of two connected components of  $\{y_b < y < y_t\} - G$ .*

We are now ready to start our construction of a drawing of  $C^*$ .

Select a point inside each connected components of the set  $\{y_b < y < y_t\} - G$ . We call  $\mathcal{N}^*$  this set of points.

For each edge of  $G$  that is clogged, we draw exactly one edge of  $C^*$  as follows. Let  $e$  be a clogged edge of  $G$ . Observations 2.3.2 and 2.3.4 imply that  $e$  is included in the boundary of two connected components of  $\{y_b < y < y_t\} - G$ . Let  $a^*$  and  $b^*$  be the points of  $\mathcal{N}^*$  that are included in these components. We draw exactly one edge  $e^*$  of  $C^*$  connecting  $a^*$  and  $b^*$  in such a way that  $e^*$  intersects  $e$  in exactly one point and  $e^*$

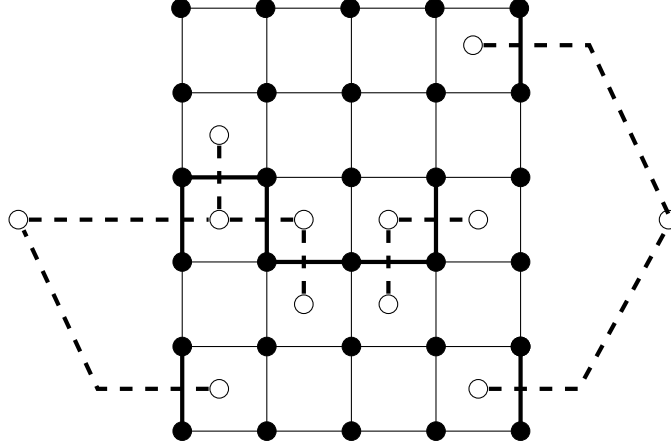


**Figure 5:** The clogged edges are thick solid lines. The open edges are thin solid lines. The thick dashed lines are the edges in  $C^*$ . The white circles are the nodes of  $C^*$ .

does not intersect any other edge of  $G$ . We say that  $e^*$  is the edge of  $C^*$  associated to  $e$ . This construction is carried out in such a way that edges of  $C^*$  may only intersect at their end points. The nodes of  $C^*$  are the end points of the edges in  $C^*$ . Note that the set of nodes of  $C^*$  is a subset of  $\mathcal{N}^*$ .

In figure 5 we show an example of a set of clogged edges and the associated  $C^*$ . The clogged edges are the thick solid lines and the edges of  $C^*$  are the dashed lines. The white circles are the nodes of  $C^*$ .

### 2.3.5 Bounding the number of clogged edges

The next sequence of observations will allow us to bound the number of clogged edges.

**Observation 2.3.5.** *The number of clogged edges is equal to the number of edges in  $C^*$ .*

This last observation is an immediate consequence of the definition of  $C^*$ .

**Observation 2.3.6.**  *$C^*$  does not have any bounded faces.*

*Proof.* By contradiction. Assume  $\Omega$  is a bounded face of  $C^*$ . From the definition of  $C^*$ , the edges of  $G$  that intersect  $C^*$  are clogged. Thus, all the edges of  $G$  that intersect  $\partial\Omega$  are clogged. Note also that  $\bar{\Omega}$ , the closure of  $\Omega$ , does not intersect any

of the exterior edges of  $G$ ,  $\partial\Omega$ , the boundary of  $\Omega$ , does not contain any node of  $G$ , and the number of edges of  $G$  that intersect  $\partial\Omega$  is positive.

The above paragraph is in contradiction of the point 3 of observation 2.3.1. Thus,  $C^*$  does not have any bounded faces.  $\square$

As a consequence, the only face of  $C^*$  is its unbounded face. Thus, we have

**Observation 2.3.7.**  *$C^*$  has only one face.*

Due to the definition of  $C^*$ , we also have the following observation.

**Observation 2.3.8.** *Let  $n_{C^*}$  be the number of nodes of  $C^*$ . Then,  $n_{C^*} \leq f_G + 1$ , where  $f_G$  is the number of faces of  $G$ .*

We are now ready to bound the number of clogged edges. Let  $n_{C^*}$ ,  $e_{C^*}$ ,  $f_{C^*}$  and  $\ell_{C^*}$  be the number of nodes, edges, faces and connected components of  $C^*$ . Euler's formula implies

$$e_{C^*} = n_{C^*} + f_{C^*} - \ell_{C^*} - 1. \quad (6)$$

From observation 2.3.7 we have  $f_{C^*} = 1$ . Thus, equation (6) reduces to

$$e_{C^*} = n_{C^*} - \ell_{C^*}. \quad (7)$$

As a consequence, using observation 2.3.8 we have

$$e_{C^*} \leq f_G + 1 - \ell_{C^*}, \quad (8)$$

where  $f_G$  is the number of faces of  $G$ . Finally, since  $\ell_{C^*} \geq 1$  and  $e_{C^*}$  is the number of clogged edges, we obtain our bound that we summarize in the following theorem.

**Theorem 1.** *Let  $G$  be a multigraph that corresponds to one of our filters. Then,*

$$\#\{\text{clogged edges}\} \leq \#\{\text{faces of } G\}. \quad (9)$$

## 2.4 Optimality of the bound

As always,  $G$  is the multigraph of one of our filters.

**Definition 5.** *We say that  $e_1, e_2, \dots, e_s$  is a feasible sequence of edges if, for each  $1 \leq i \leq s$ , there is flow through the edge  $e_i$  when  $e_1, e_2, \dots, e_{i-1}$  are clogged and all the other edges are open. We say that  $s$  is the length of the sequence.*

Recall that an edge can clog only when suspension flows through it. Thus, if  $q$  edges clogged, and the  $i^{\text{th}}$  edge that clogged was  $e_i$ , then  $e_1, e_2, \dots, e_q$  is a feasible sequence of edges. Note that the bound of section 2.3 is actually a bound on the length of feasible sequences of edges.

In this section we will show that, if every interior edge of  $G$  is contained in a percolating path, our bound is sharp (see definition 1 for a reminder of the meaning of interior edge). In other words, there exists a feasible sequence of edges whose length is equal to our bound, the number of faces of  $G$  (the right hand side of equation (9)).

Let  $e$  be an interior edge of  $G$ . As illustrated in figure 4 and previously discussed, if there is no percolating path that contains  $e$ , then the pressure at the end points of  $e$  are equal which implies that there is no flow through  $e$  and thus,  $e$  can never clog. Removing first all such edges from  $G$ , then all the exterior edges, then the nodes that are left isolated, and finally adding new exterior edges as necessary, leads to a new multigraph  $\tilde{G}$  for which the bound will be attained. Note that the flow in  $G$  is exactly equal to the flow in  $\tilde{G}$ . There is no flow within edges of  $G$  that do not belong to  $\tilde{G}$ .

The number of channels, which ones, and the order in which they actually clog depend on many factors and it is not our goal here to make those predictions. In particular, while the length of the longest feasible sequence of edges is an upper bound on the number of channels that actually clog, these numbers may not be equal. We will come back to this issue in section 2.6.

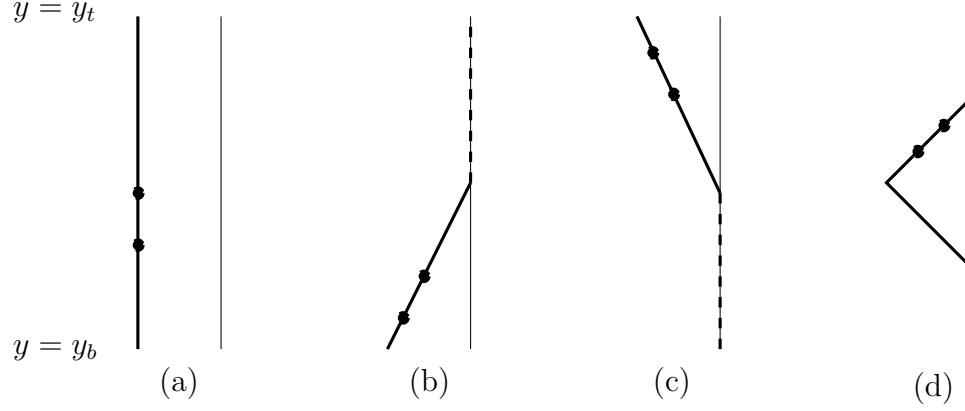


**Figure 6:** The four different possibilities of observation 2.4.1. We do not show all the multigraph  $G$ , only  $e$ ,  $\bar{Q}$  and  $P$ . The edge  $e$  is the segment between the solid small circles.  $P$  is the thin solid vertical line,  $\bar{Q}$  the thick solid line, and  $R$  the union of  $\bar{Q}$  and the dashed lines.

### 2.4.1 Left most percolating paths

**Observation 2.4.1.** *Let  $P = n_0, e_1, n_1, \dots, e_r, n_r$  be a percolating path. Let  $e$  be an edge to the left of  $P$ . If  $e$  is included in a percolating path, then there exists a percolating path  $R$  such that  $P$  and  $e$  are to the right of  $R$ .*

*Proof.* Assume  $e$  is not in  $P$  since otherwise the observation is trivially true by selecting  $R = P$ . Let  $Q$  be a percolating path that contains  $e$ . Let  $\bar{Q}$  be the largest path that satisfies: 1)  $\bar{Q}$  is included in  $Q$ , 2)  $\bar{Q}$  contains  $e$ , 3)  $\bar{Q}$  is to the left of  $P$  and 4)  $\bar{Q}$  may only intersect  $P$  at the end points of  $\bar{Q}$ .

If  $\bar{Q} = Q$ , as in figure 6 (a), select  $R = Q$ . Note that  $e$  and  $P$  are to the right of  $R$ . Otherwise,  $\bar{Q}$  intersects  $P$ . In this case,  $\bar{Q} \cap P$  splits  $P$  in two or three connected sections. Replacing one of these connected sections with  $\bar{Q}$  leads to the percolating path  $R$  we are looking for. If  $\bar{Q}$  contains a bottom exterior node, as in figure 6 (b), we replace the section of  $P$  that has a bottom exterior node. If  $\bar{Q}$  contains a top exterior node, as in figure 6 (c), we replace the section of  $P$  that has a top exterior node. If  $\bar{Q}$  does not contain any exterior node, as in figure 6 (d), we replace the section of  $P$  without exterior nodes.  $\square$

This last observation and the fact that each exterior node is the end point of an interior node, lead to the following:

**Observation 2.4.2.** *If every interior edge in  $G$  is included in a percolating path, then there is a unique percolating path  $P$  in  $G$  such that  $G$  is to the right of  $P$ . We call  $P$  the left most percolating path of  $G$ .*

### 2.4.2 First edge of a feasible sequence of edges

Assume that every interior edge in  $G$  is included in a percolating path. Our goal is to construct a feasible sequence of edges  $e_1, e_2, \dots, e_N$  of maximum length. Let  $P$  be the left most percolating path of  $G$ . In this subsection we identify  $\bar{P}$ , a subpath of  $P$ , from where  $e_1$  will be selected. The selection of  $\bar{P}$  is done with care so that the rest of the sequence,  $e_2, \dots, e_N$ , can be constructed inductively as we will do in the next subsection.

**Observation 2.4.3.** *Assume that every interior edge in  $G$  is included in a percolating path of  $G$ . Let  $P$  the left most percolating path of  $G$ . Assume that there are no bounded faces  $F$  of  $G$  such that  $\partial F \cap P$  contains an edge. Then  $P = G$ .*

*Proof.* By contradiction. Assume  $P \neq G$ . Then, there exists an edge in  $G$  not in  $P$ . In fact, since every exterior node is the end point of an interior edge, we have that there exists an interior edge  $e$  in  $G$  such that  $e$  is not in  $P$ . Let  $Q$  be a percolating path in  $G$  containing  $e$ . Note that there is a non-empty open bounded  $\Omega$  enclosed by  $P, Q, y = y_b$  and  $y = y_t$ . Note also that at least one edge of  $P$  is in the boundary of  $\Omega$ . The closure of  $\Omega$  is the union of the closure of the bounded faces of  $G$  included in  $\Omega$ . Thus, there exists  $F$ , a bounded face of  $G$ , such that  $\partial F \cap P$  contains an edge. This is a contradiction, which proves the observation. □

**Observation 2.4.4.** *Assume that every interior edge in  $G$  is included in a percolating path of  $G$ . Let  $F$  be a bounded face of  $G$ . Then,  $\partial F \cap \{y = y_b\}$  is connected and  $\partial F \cap \{y = y_t\}$  is also connected.*

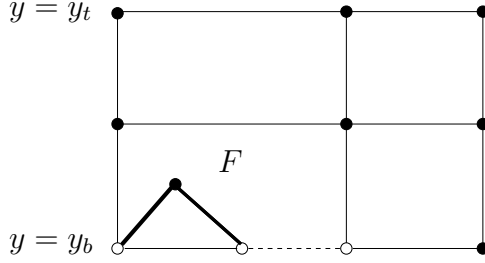


**Figure 7:** Multigraph  $G$ .  $\partial F \cap \{y = y_b\}$  is the edge in dashed line and the white nodes, which is a disconnected set. The thick solid line is  $\bar{Q}$ . The edges in  $\bar{Q}$  are not included in any percolating path of  $G$ .

*Proof.* Assume that  $\partial F \cap \{y = y_b\}$  is not connected. Then, as illustrated in figure 7, there is a path  $\bar{Q}$  that is included in  $\partial F$  such that  $\bar{Q} \cap \{y = y_b\}$  are the end points of  $\bar{Q}$ . As it is also clear from that figure, the edges in  $\bar{Q}$  are interior edges and none of them is included in a percolating path of  $G$ , which contradicts our assumption. Thus,  $\partial F \cap \{y = y_b\}$  is connected. Analogously,  $\partial F \cap \{y = y_t\}$  is also connected.  $\square$

**Observation 2.4.5.** *Assume that every interior edge in  $G$  is included in a percolating path of  $G$ . Let  $P$  be the left most percolating path of  $G$ . Assume that  $G$  has a bounded face. Then, there exists  $F$ , a bounded face of  $G$ , such that:*

1.  $\partial F \cap P$  contains an edge and,
2.  $\partial F \cap (P \cup \{y = y_t\} \cup \{y = y_b\})$  is connected.

*Proof.* Let  $S$  be the path that results from the following steps. We start at the right most exterior node of the bottom boundary and walk left along that boundary toward the path  $P$ . We continue walking through  $P$  to the top boundary. We then walk right along the top boundary and end the path at the right most exterior node of the top boundary (see figure 8).

Since  $G$  has a bounded face,  $P \neq G$  and thus, from observation 2.4.3, there exists  $F_0$ , a bounded face of  $G$ , such that  $\partial F_0 \cap P$  contains an edge. Let  $S_{F_0} = \partial F_0 \cap S$  and  $\bar{S}_{F_0}$  be the smallest path included in  $S$  that contains  $S_{F_0}$ . Recall that paths are connected. Thus, if  $\bar{S}_{F_0} = S_{F_0}$ , then  $F = F_0$  is a face we are looking for.

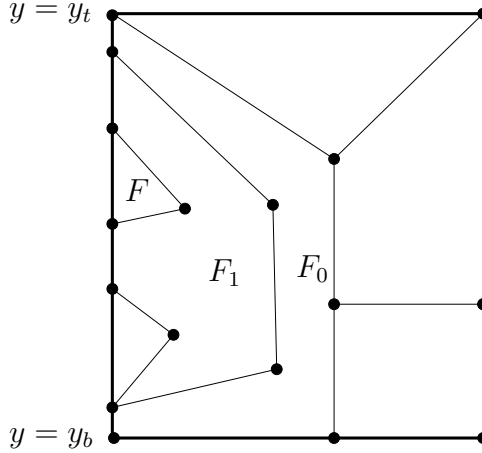


**Figure 8:** Multigraph  $G$ . The edges of the path  $S$  are in thick lines. Example of a sequence  $F_0, F_1, F_2 = F$  constructed as in observation 2.4.5.

We next show that  $P \cap \bar{S}_{F_0} \subseteq S_{F_0}$  implies that  $\bar{S}_{F_0} = S_{F_0}$ . Assume that  $P \cap \bar{S}_{F_0} \subseteq S_{F_0}$ . If both  $\partial F_0 \cap \{y = y_b\}$  and  $\partial F_0 \cap \{y = y_t\}$  are empty sets, then  $\bar{S}_{F_0} = P \cap \bar{S}_{F_0} \subseteq S_{F_0}$ . Assume now that  $\partial F_0 \cap \{y = y_b\}$  is non-empty. Thus,  $\bar{S}_{F_0}$  contains the exterior node of  $P$  in the bottom boundary and since  $P \cap \bar{S}_{F_0} \subseteq S_{F_0}$ , that exterior node is also in  $S_{F_0}$ . Thus,  $\{y = y_b\} \cap S_{F_0} = \partial F_0 \cap \{y = y_b\}$  also contains that exterior node and, given that  $\partial F_0 \cap \{y = y_b\}$  is connected due to observation 2.4.4, we have that  $\{y = y_b\} \cap \bar{S}_{F_0} \subseteq S_{F_0}$ . This argument applied to the top boundary leads to  $\bar{S}_{F_0} = (P \cup \{y = y_t\} \cup \{y = y_b\}) \cap \bar{S}_{F_0} \subseteq S_{F_0}$  if  $(P \cap \bar{S}_{F_0}) \subseteq S_{F_0}$ .

We are left to show that the observation is true when  $\bar{S}_{F_0} \neq S_{F_0}$  (see figure 8) and so, we now assume  $\bar{S}_{F_0} \neq S_{F_0}$ . Given the above paragraph, we have that  $\bar{S}_{F_0} - S_{F_0}$  intersects  $P$  in at least one edge, say  $e$ . As illustrated in figure 5, we can select  $F_1$ , a bounded face of  $G$ , such that  $\partial F_1$  contains  $e$ . Let  $S_{F_1} = \partial F_1 \cap S$  and  $\bar{S}_{F_1}$  the smallest path included in  $S$  that contains  $S_{F_1}$ . If  $\bar{S}_{F_1} = S_{F_1}$ , then  $F = F_1$  is a face we are looking for. Otherwise, we note that  $\bar{S}_{F_1}$  is included in a connected component of  $\bar{S}_{F_0} - S_{F_0}$  and thus,  $\bar{S}_{F_1} \subsetneq \bar{S}_{F_0}$ . As a consequence, since  $G$  is a finite multigraph, repeating this procedure as many times as necessary we will find the face  $F$  we are looking for (see figure 8). □

Assume that every interior edge in  $G$  is included in a percolating path. Let  $F$  be a bounded face of  $G$  that satisfies the conditions of observation 2.4.5. Let  $\bar{P} = P \cap \partial F$ , where  $P$  is the left most percolating path of  $G$ . In the next subsection we will show how to construct a feasible sequence of edges  $e_1, e_2, \dots, e_N$  of maximum length where  $e_1$  will be selected from  $\bar{P}$ .

### 2.4.3 Feasible sequence of edges of maximal length

**Observation 2.4.6.** *Assume that every interior edge in  $G$  is included in a percolating path. Let  $P$  be the left most percolating path of  $G$ . Assume that  $G$  has a bounded face. Let  $F$  be a face of  $G$ , such that: 1)  $\partial F \cap P$  contains an edge and, 2)  $\partial F \cap (P \cup \{y = y_t\} \cup \{y = y_b\})$  is connected.*

*Then, for every interior edge  $e$  in  $G$  not in  $\partial F \cap P$  there exists a percolating path  $Q$  of  $G$  such that  $Q$  contains  $e$  and  $Q$  does not have any edge in  $\partial F \cap (P \cup \{y = y_t\} \cup \{y = y_b\})$ .*

*Proof.* Let  $S_1$  be the section of  $P$  that does not intersect  $\partial F$ , i.e.  $S_1 = P - \partial F$ . Let  $S_2$  be the section of  $\partial F$  that does not intersect neither  $P$  nor the boundaries, i.e.  $S_2 = \partial F - (P \cup \{y = y_t\} \cup \{y = y_b\})$ . Let  $S$  be the percolating path that results from walking along  $S_1 \cup S_2$  (see figure 9). Note that every edge in  $G$  not in  $\partial F \cap (P \cup \{y = y_t\} \cup \{y = y_b\})$  is to the right of  $S$ .

Let  $e$  be an interior edge in  $G$  not in  $\partial F \cap P$ . Let  $R$  be a percolating path of  $G$  that contains  $e$ . Let  $\bar{Q}$  be the largest subpath of  $R$  that contains  $e$  such that  $\bar{Q}$  may only intersect  $S$  at the end points of  $\bar{Q}$ . As illustrated in figure 10, we can construct a percolating path  $Q$  that contains  $\bar{Q}$ , may contain sections of  $S$ , but does not contain any edge outside  $\bar{Q} \cup S$ . Thus,  $Q$  contains  $e$  and does not have any edge in  $\partial F \cap (P \cup \{y = y_t\} \cup \{y = y_b\})$ .  $\square$

**Observation 2.4.7.** *Assume that every interior edge in  $G$  is included in a percolating path of  $G$ . Let  $P$  be the left most percolating path of  $G$ . Assume that  $G$  has a bounded*

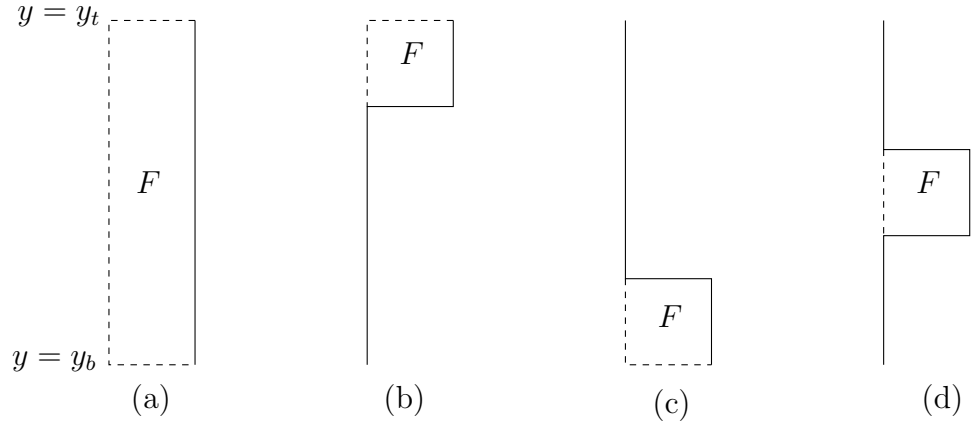


**Figure 9:** Four different possibilities of  $F$  from observation 2.4.6 and theorem 2. The solid line is the percolating path  $S$  of observation 2.4.6. The left vertical line is  $P$ .  $P \cap S$  is in solid line and the section of  $P$  that does not intersect  $S$  is in dashed line. The dashed horizontal lines are the sections of the top and bottom boundary that are to the left of  $S$ .

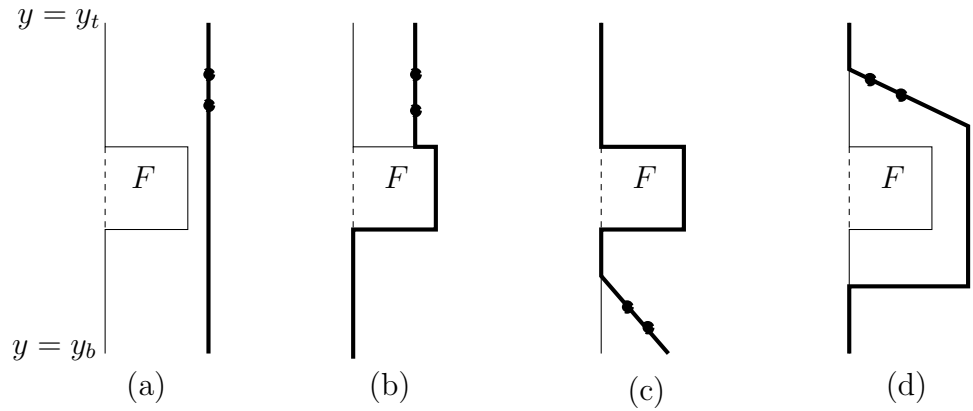


**Figure 10:** Four different possibilities of the percolating path  $Q$ , in thick solid lines, from observation 2.4.6. The edge  $e$  is between the solid small circles. The left vertical line is  $P$ .

face. Let  $F$  be a bounded face of  $G$ , such that: 1)  $\partial F \cap P$  contains an edge and, 2)  $\partial F \cap (P \cup \{y = y_t\} \cup \{y = y_b\})$  is connected. Let  $G'$  be the multigraph that results from first removing from  $G$  the edges in  $\partial F \cap (P \cup \{y = y_t\} \cup \{y = y_b\})$ , and then removing the nodes that are left isolated. Then:

1. Every interior edge in  $G'$  is included in a percolating path in  $G'$ .
2.  $f_{G'} = f_G - 1$ , i.e. the number of faces of  $G'$  is equal to the number of faces of  $G$  minus one.
3.  $G'$  is the multigraph of one of our filters.

*Proof.* Point 1 is an immediate consequence of observation 2.4.6.

Point 2 results from the simple facts that: 1) all the bounded faces of  $G'$  are bounded faces of  $G$ , 2) the only bounded face of  $G$  that is not a face of  $G'$  is  $F$ , and 3) both  $G$  and  $G'$  (as well as any multigraph) have only one unbounded face (note that  $G'$  results from removing the dashed lines in figure 9).

Point 3 is also clear. □

**Theorem 2.** *If every interior edge in  $G$  is included in a percolating path of  $G$ , then there exist a feasible sequence of edges of length  $f_G$ . Thus, our bound is optimal for this class of filters.*

*Proof.* We will prove the theorem by induction on  $f_G$ . First note that  $f_G = 1$  if and only if  $G$  is a percolating path. In this case, any edge of  $G$  forms a feasible sequence of edges of length  $f_G = 1$ .

Assume now that  $f_G > 1$ . Let  $P$  be the left most percolating path of  $G$ . Note that  $P$  can not be equal to  $G$  since otherwise  $f_G$  would be equal to one.

Let  $F$  be a bounded face of  $G$ , such that: 1)  $\partial F \cap P$  contains an edge and, 2)  $\partial F \cap (P \cup \{y = y_t\} \cup \{y = y_b\})$  is connected. Such a face exists by the observations of this section. Let  $e_1$  be any edge in  $\partial F \cap P$ .

Let  $G'$  be the multigraph that results from first removing from  $G$  the edges in  $\partial F \cap (P \cup \{y = y_t\} \cup \{y = y_b\})$ , and then removing the nodes that are left isolated. From observation 2.4.7, every interior edge in  $G'$  is included in a percolating path in  $G'$ ,  $f_{G'} = f_G - 1$  and  $G'$  is the multigraph of one of our filters.

By inductive hypothesis there exists in  $G'$  a feasible sequence of edges of length  $f_{G'} = f_G - 1$ . For convenience, call one such sequence  $e_2, \dots, e_{f_G}$ . From the observations of this section, it follows that  $e_1, e_2, \dots, e_{f_G}$  is a feasible sequence of edges in  $G$  which proves the theorem.  $\square$

## 2.5 *The bound in terms of the average degree of $G$ for large filters*

As always,  $G$  is a multigraph of one of our filters. We assume in this section that every interior edge of  $G$  is contained in a percolating path. We recall that  $f_G$ ,  $e_G$  and  $n_G$  are the numbers of faces, edges and nodes of  $G$  respectively. We also recall that  $d_G$ , the average degree of  $G$ , is given by  $d_G = 2e_G/n_G$  (equation (2)).

Assume that the number of edges is large, i.e.  $e_G \gg 1$ . In this case, the Euler formula  $f_G + n_G = e_G + \ell_G + 1$  reduces to  $f_G + n_G \approx e_G$  since  $\ell_G \approx 1$ . Thus, from equation (2), and if  $d_G \neq 2$ , we have  $f_G + 2e_G/d_G \approx e_G$ . This leads to the following observation.

**Observation 2.5.1.** *If  $e_G \gg 1$ , then our bound (9) reads*

$$\#\{\text{clogged edges}\} \lesssim \frac{d_G - 2}{d_G} e_G. \quad (10)$$

*In particular, if every interior edge of  $G$  is contained in a percolating path, the number of edges in a feasible sequence of edges with maximum length is asymptotically  $((d_G - 2)/d_G)e_G$ .*

In many situations of interest,  $G$  is a graph, i.e. no two edges have the same end points. For example, if all the edges in a multigraph are straight segments, then the

multigraph is really a graph. It is a well known fact from graph theory that, if  $G$  is a planar graph, the average degree of  $G$  is bounded by 6, i.e.  $d_G \leq 6$ . This leads to the following observation.

**Observation 2.5.2.** *If  $G$  is a graph and  $e_G \gg 1$ , then*

$$\#\{\text{clogged edges}\} \lesssim \frac{2}{3} \#\{\text{all edges}\}. \quad (11)$$

A natural goal is to design filters that use as much of the void space as possible to trap particles before the filter ceases to be permeable. Thus, of particular interest is to know the proportion of channels that are clogged when the filter ceases to be permeable. The last observation provides a bound on this quantity whenever  $G$  is a graph.

As particular examples, consider the graphs of figure 11. At this point do not make a distinction between solid and dashed edges. In the large filter limit, i.e. the distance between the top and bottom boundaries is much larger than the length of the edges, the graph with square bounded faces satisfies  $d_G \approx 4$  and thus, for this graph, equation (10) implies  $\#\{\text{clogged edges}\} \lesssim e_G/2$ . For the graph with triangle bounded faces, we have  $d_G \approx 6$  and thus,  $\#\{\text{clogged edges}\} \lesssim 2e_G/3$ . For the graph with hexagonal bounded faces, we have  $d_G \approx 3$  and thus,  $\#\{\text{clogged edges}\} \lesssim e_G/3$ .

## ***2.6 A subclass of filters and examples***

In this section, we consider filters in which every interior edge is included in a percolating path. We have shown that, for this kind of filters, our bound is sharp, i.e. there is a feasible sequence of edges whose number of edges or length is equal to our bound, i.e. the number of faces of the multigraph (see right hand side of equation (9)). However, in general, there are many feasible sequences of edges that make the filter non-permeable and the length of most of them is less than our bound. Thus, the feasible sequence of edges that is realized, i.e. the sequence of edges that actually

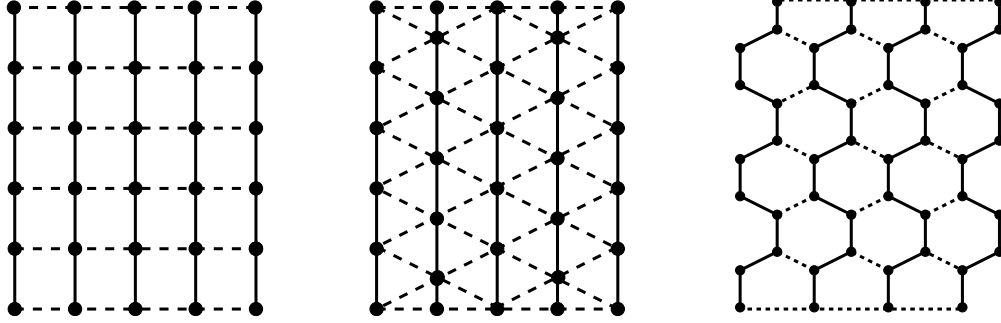


**Figure 11:** Multigraphs with geometries of class  $\mathcal{A}$ . The percolating paths  $P_i$  are in solid lines. The crossing paths  $H_{i,j}$  are in dashed lines.

clog and make the filter non-permeable, which depends on the flow conditions as well as the width of the channels, is, in general, much shorter than the feasible sequences of edges with maximum length.

In this section, we will restrict our attention to a subclass of filters for which we will show how to select the width of the channels so that, as suspension flows, the feasible sequence of edges that is realized and make the filter non-permeable will indeed have maximum length.

### 2.6.1 Subclass of filters. The geometries

**Definition 6.** We say that a multigraph  $G$  that corresponds to one of our filters has geometry of class  $\mathcal{A}$  if there is a non-negative integer  $r$  and a sequence of disjoint percolating paths  $P_0, P_1, \dots, P_r$  in  $G$  such that, for each  $i$ ,  $0 \leq i < r$

1.  $P_i$  is to the left of  $P_{i+1}$ .
2. There are positive integers  $s_i$  such that  $P_i$  and  $P_{i+1}$  are joined by  $s_i + 1$  paths that may only have end points in common, i.e. for each  $j$ ,  $0 \leq j \leq s_i$ , there is a path  $H_{i,j}$  such that: 1)  $H_{i,j} \cap P_i$  is an end point of  $H_{i,j}$ , 2)  $H_{i,j} \cap P_{i+1}$  is the other end point of  $H_{i,j}$  and 3)  $H_{i,j_1}$  and  $H_{i,j_2}$  may only intersect at their end points if  $j_1 \neq j_2$ .
3.  $G$  is the union of the percolating paths  $P_i$  ( $0 \leq i \leq r$ ) and the “crossing” paths

$$H_{i,j} \quad (0 \leq i < r, 0 \leq j \leq s_i).$$

For convenience, we assume that the path  $H_{i,j}$  are labeled in such a way that  $H_{i,j+1}$  is above  $H_{i,j}$  ( $0 \leq i < r, 0 \leq j < s_i$ ). More precisely,  $H_{i,j+1}$  is in the closure of the bounded region whose boundary is included in  $\{y = y_t\} \cup P_i \cup P_{i+1} \cup H_{i,j}$ . Note that  $H_{i,0}$  is included in the bottom boundary and  $H_{i,s_i}$  is included in the top boundary.

Examples of multigraphs that have geometry of class  $\mathcal{A}$  are shown in figure 11. The percolating paths  $P_i$  are in solid lines. The crossing paths  $H_{i,j}$  are in dashed lines.

### 2.6.2 Subclass of filters. The width of the channels

The physical mechanisms that lead to the clogging of channels may be complex and depend on the particular problem under consideration. Here we will assume the following simple rules. Each channel is either thin or thick. Thick channels never clog and thin channels eventually clog if there is flow through them.

We now select the thin and thick edges. Let  $G$  be a multigraph that has geometry of class  $\mathcal{A}$ . Let  $P_0, P_1, \dots, P_r$  be the percolating paths as in definition 6. Every percolating path is split into subpaths by the crossing paths. For  $i$  even, let  $\bar{P}_i$  be the subpath of  $P_i$  that contains an exterior node at the top boundary. For  $i$  odd, let  $\bar{P}_i$  be the subpath of  $P_i$  that contains an exterior node at the bottom boundary. One edge in each of the subpaths  $\bar{P}_i$  for any  $i$  is selected to be thin. One edge in each of the crossing paths  $H_{i,j}$  is also selected to be thin. Every other edge is chosen thick. In figures 12 we show the multigraphs of figure 11 but now the thick edges are in solid lines and the thin edges in dashed lines.

**Definition 7.** *We say that a multigraph  $G$  that corresponds to one of our filters is of class  $\mathcal{A}$  if  $G$  has geometry of class  $\mathcal{A}$  and the width of the edges of  $G$  are selected as described above.*

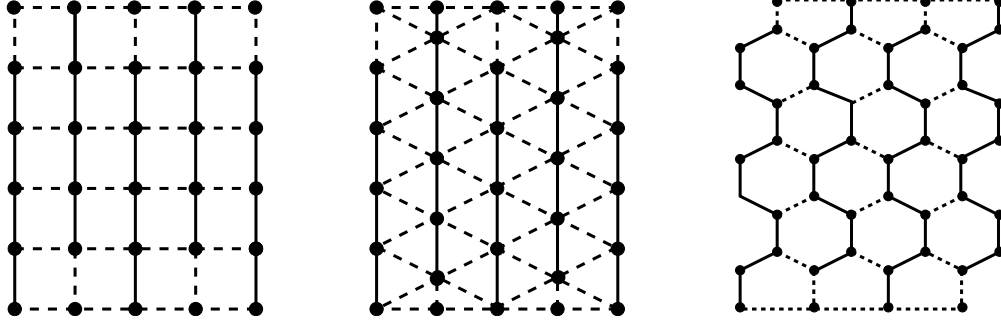


**Figure 12:** Multigraphs of figure 11. The thick edges are in solid lines. Thin edges in dashed lines.

### 2.6.3 The bound realizes for filters of class $\mathcal{A}$

We now show that, for the filters considered in this section, i.e. with multigraph of class  $\mathcal{A}$ , the bound realizes, i.e. the number of edges that actually clog is equal to our bound, the number of faces of the multigraph of the filter. We show this in two steps. We first show that in each of the paths  $\bar{P}_i$  the thin edge clogs and in each of the paths  $H_{i,j}$  not included in the top or bottom boundaries, i.e.  $H_{i,j}$  for  $1 \leq j < s_i$  the thin edge also clogs. Then, we show that the number of these paths is equal to the number of faces of the multigraph of the filter.

**Observation 2.6.1.** *In each of the paths  $\bar{P}_i$  ( $0 \leq i \leq r$ ) the thin edge clogs and in each of the paths  $H_{i,j}$  not included in the top or bottom boundaries ( $0 \leq i < r, 1 \leq j < s_i$ ), the thin edge clogs.*

*Proof.* Let  $e_i$  be the thin edge in  $\bar{P}_i$ . All the other edges in  $P_i$  are thick and thus, they never clog. As a consequence, while  $e_i$  is open, there will be flow through the whole percolating path  $P_i$  and in particular through  $e_i$ . This implies that eventually  $e_i$  clogs.

Let  $H_{i,j}$  be one of the crossing paths not included in the top or bottom boundaries, i.e.  $1 \leq j < s_i$ . We connect one end point of  $H_{i,j}$  to a bottom exterior node and the other to a top exterior node with paths of thick edges as follows. Let  $Q$  be the subpath of  $P_i$  that has an exterior node as an end point, shares the other end point

with  $H_{i,j}$  and all the edges in  $Q$  are thick. Let  $R$  be the subpath of  $P_{i+1}$  that has an exterior node as an end point, shares the other end point with  $H_{i,j}$  and all the edges in  $R$  are thick. From the discussion of section 2.6.1 and section 2.6.2, it is clear that  $Q$  and  $R$  are well defined. It is also clear that the union of  $Q$ ,  $R$  and  $H_{i,j}$  form a percolating path whose only thin edge is the one in  $H_{i,j}$ . This implies that the thin edge in  $H_{i,j}$  eventually clogs.  $\square$

**Observation 2.6.2.** *The number of the paths  $\bar{P}_i$  ( $0 \leq i \leq r$ ) and  $H_{i,j}$  not included in the top or bottom boundaries ( $0 \leq i < r, 1 \leq j < s_i$ ) is equal to  $f_G$ , the number of faces of  $G$ .*

*Proof.* We first note that, the number of the paths  $\bar{P}_i$  ( $0 \leq i \leq r$ ) and  $H_{i,j}$  not included in the top or bottom boundaries ( $0 \leq i < r, 1 \leq j < s_i$ ) is equal to  $1+r+\sum_{i=0}^{r-1}(s_i-1) = 1+\sum_{i=0}^{r-1} s_i$ . Thus our goal reduces to show that  $f_G = 1+\sum_{i=0}^{r-1} s_i$ .

Let  $0 \leq i < r$  and  $1 \leq j \leq s_i$ . If we remove from the plane the paths  $P_i$ ,  $H_{i,j-1}$ ,  $P_{i+1}$  and  $H_{i,j}$ , we are left with one bounded and one unbounded connected component. Let  $F_{i,j}$  be the bounded component. It is clear that the bounded faces of  $G$  are  $F_{i,j}$  for  $0 \leq i < r$  and  $1 \leq j \leq s_i$ . Therefore,  $f_G = 1 + \sum_{i=0}^{r-1} s_i$ , which completes the proof.  $\square$

#### 2.6.4 Building filters of class $\mathcal{A}$ from thin filters

We now discuss a possible mean, at least theoretically, to construct filters of class  $\mathcal{A}$ .

We start with a thin filter with thin channels. By a thin filter we mean that the corresponding graph is the union of disjoint percolating paths connected only by the top and bottom boundaries. An example is shown in the top figure of figure 13.

Next, we fold the thin filter as shown in the middle figure of figure 13. As we compress the folded filter from the sides, the spaces between folds become the thick channels and we are left with the new filter shown in the bottom figure of figure 13. The applied pressure in the folding step should be high, but not so high so the new

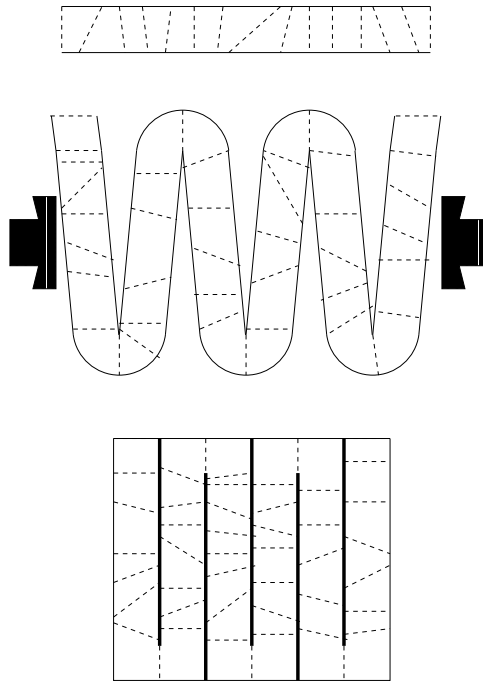


**Figure 13:** Building a filter of class  $\mathcal{A}$ . In the top figure we start with a thin filter with thin channels. In the middle figure we fold the thin filter. The bottom figure shows the resulting filter after folding and compressing. The thick edges are in solid thick lines. The thin edges are in dashed lines.

pore space, the thick channels, are in fact thicker than the channels in the original thin filter before folding. The resulting filter is a filter of class  $\mathcal{A}$ .

Note that the above discussion suggest a way to construct filters of *long life* even if the original thin filter does not strictly satisfy the condition of having the corresponding graph be the union of disjoint percolating paths.

### 2.6.5 Further comments on filters of class $\mathcal{A}$

As channels clog, the permeability of the filter decreases. This is unavoidable. Nevertheless, we expect that this decrease in permeability will be relatively slow (as comparing with other filters) for filters of class  $\mathcal{A}$ . The reason being is that suspension can flow with relative ease along the thick channels and, as shown in the proof of observation 2.6.1, this family of filters have lots of percolating paths where all but one edge are thick.

In chapter 4, we run numerical simulations of filter realizations. To do these simulations further modeling is needed, which is discussed in the first sections of chapter 4. The simulations show an optimal performance for class  $\mathcal{A}$  filters. The bound in the number of channels that clog is attained, no particle crosses through the filter without being trapped and the life average flow rate of the filter is high.

## CHAPTER III

### PLUGGING OF POROUS MEDIA NEAR WELLS

Fluid in porous media flows through tortuous paths, i.e. paths that are not straight. This tortuosity and inertial effects cause fines to collide with pore walls. After each collision, a particle loses momentum and needs to be accelerated again by the fluid through hydrodynamic forces. As a result, the average velocity of fines is smaller than that of the fluid.

To simplify the discussion that will follow, we now introduce some notation. We will denote by  $\mathbf{v}$  what we call the *macroscopic* fluid velocity, i.e.  $\mathbf{v}$  is the average of the fluid velocity in regions much larger than the pores but much smaller than the material. Note that, in principle,  $\mathbf{v}$  is a function of the spatial position  $\mathbf{x}$  and time  $t$ , i.e.  $\mathbf{v} = \mathbf{v}(\mathbf{x}, t)$ . We denote by  $\mathbf{u}$  the *macroscopic* fines velocity, i.e.  $\mathbf{u}$  is the average of the velocities of the fines in regions much larger than the pores but much smaller than the material. Note that, according with the discussion of the above paragraph,  $\|\mathbf{u}(\mathbf{x}, t)\| \leq \|\mathbf{v}(\mathbf{x}, t)\|$ , where  $\|\mathbf{u}(\mathbf{x}, t)\|$  denotes the euclidean norm of the vector  $\mathbf{u}(\mathbf{x}, t)$ .

If the macroscopic fluid velocity is spatially homogeneous, i.e.  $\mathbf{v}$  is independent of  $\mathbf{x}$ , the macroscopic fines velocity  $\mathbf{u}$  will also be independent of  $\mathbf{x}$ . Thus, the location of the maximum concentration of fines in space will travel at velocity  $\mathbf{u}$  but the concentration value will not change. On the other hand, if  $\mathbf{v}$  is not independent of  $\mathbf{x}$ ,  $\mathbf{u}$  will not be independent of  $\mathbf{x}$  either. As a consequence, both the location and the value of the maximum concentration of fines in space will change with time. In particular, the concentration of fines may exceed some critical value that leads to the clogging of pore throats and eventually the plugging of the medium. Motivated by the

clogging that is sometimes observed in petroleum and water wells, we will consider two-dimensional macroscopic flows with circular symmetry. Clearly, the macroscopic fluid velocity is not spatially homogeneous in this case, it decays with the distance to the well.

In section 3.1, we introduce a pore-scale mathematical model that allow us to obtain the macroscopic fines velocity  $\mathbf{u}$  as a function of the macroscopic fluid velocity  $\mathbf{v}$ . This pore-scale model results from assuming that any given particle follows a tortuous path that consist of a sequence of straight channels of length  $L$  and that, each time that a particle reaches the end of a channel, it collides with the pore wall and losses all its momentum. Thus, each time the particle enters a new channel, it starts traveling through the channel with an initial velocity equal to zero and it accelerates due to hydrodynamic forces.

In section 3.2, we introduce a macro-scale mathematical model that describes the time evolution of concentration of fines. This model results from the fact that the concentration of fines is convected with velocity  $\mathbf{u}$ . We also propose that regions of the medium plug if and when the concentrations of fines in those regions exceed a certain critical value.

The rest of this chapter is organized as follows: In section 3.3 we explain some qualitative features of our model. In section 3.4 we introduce our criterion to determine which regions of the medium clog and when. In section 3.5 we study the behavior of our model and in section 3.6 we conclude with some discussions.

### ***3.1 Macroscopic fines velocity as function of the macroscopic fluid velocity***

#### **3.1.1 Review. Hydrodynamic force on a spherical particle immerse in a fluid**

Assume an incompressible spherical particle with radius  $r_p$  is immersed in an incompressible Newtonian fluid that extends to infinity. Assume also that the particle

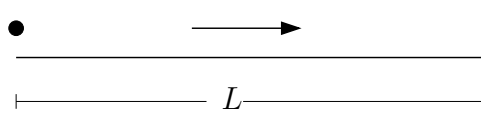


**Figure 14:** Channel of length  $L$  filled with an incompressible fluid. The arrow indicate the direction of the flow. The black circle is a particle that will move toward the right end due to hydrodynamic forces.

moves with constant velocity  $\mathbf{u}$  and the velocity of the fluid tends to the constant value  $\mathbf{v}$  far away from the particle. It is well known (see [2]) that the force the fluid exerts on the particle is

$$\mathbf{F} = 6\pi r_p \mu (\mathbf{v} - \mathbf{u}), \quad (12)$$

where  $\mu$  is the fluid viscosity.

### 3.1.2 Average velocity of a particle flowing through a straight channel when the particle is initially at rest at one end of the channel

Consider a straight channel of length  $L$  filled with an incompressible fluid, see figure 14. Assume the fluid within the channel flows from left to right at a constant speed  $v^*$ . Note that, as an approximation, we assume that the fluid velocity is constant through the channel and thus, it does not satisfy the non-slip boundary conditions at the channel walls.

If at time  $t = 0$ , we place a particle at the left end of the channel, it will move toward the right end following Newton's law. More precisely, if  $x(t)$  is the distance between the particle and the left end of the channel at time  $t$ , Newton's law implies

$$\frac{4}{3}\pi\rho_p r_p^3 x'' = F \quad \text{and} \quad x(0) = x'(0) = 0, \quad (13)$$

where  $F$  is the force the particle experiences in the direction of the channel,  $\rho_p$  and  $r_p$  are the density and radius of the particle respectively, and  $x'$  and  $x''$  are the first and second the derivatives of  $x$  with respect to  $t$ . Note that we neglect any force the particle may experience in directions perpendicular to the channel.

Keeping only hydrodynamic forces (we neglect gravity) and approximating  $F$  by the force the particle would experience if the channel width were much larger than the particle diameter, i.e. equation (12), we have  $F = 6\pi r_p \mu (v^* - x')$  and thus,

$$\frac{4}{3}\pi\rho_p r_p^3 x'' = 6\pi r_p \mu (v^* - x') \quad \text{and} \quad x(0) = x'(0) = 0, \quad (14)$$

where  $\mu$  is the viscosity of the fluid.

The above initial value problem can be solved explicitly. More precisely, defining

$$\kappa = \frac{9}{2} \frac{\mu}{\rho_p r_p^2}, \quad (15)$$

we have that

$$x(t) = v^* t - \frac{v^*}{\kappa} (1 - e^{-\kappa t}). \quad (16)$$

Let  $T$  be the time when the particle reaches the right end. Since the length of the channel is  $L$  and given equation (16), we have

$$L = v^* T - \frac{v^*}{\kappa} (1 - e^{-\kappa T}). \quad (17)$$

We denote by  $u^*$  the average speed of the particle as it travels through the channel. Our goal is to find  $u^*$  as a function of the fluid speed  $v^*$  and the parameters of the system. This relation is obtained from equation (17) once we note that  $u^* = L/T$  and replace  $T$  by  $L/u^*$  in that equation to obtain, after simple manipulations,

$$1 = \frac{v^*}{\kappa L} \left[ \frac{\kappa L}{u^*} - \left( 1 - e^{-\frac{\kappa L}{u^*}} \right) \right]. \quad (18)$$

### 3.1.3 Tortuosity of flow paths in porous media

Assume now that suspension, i.e. fluid with fines, flows within the void space of a porous medium. Let  $\mathbf{x}_f(t)$  be the path of an element of fluid. This path will not be straight, it will be tortuous. Thus, the distance traveled by the fluid element in

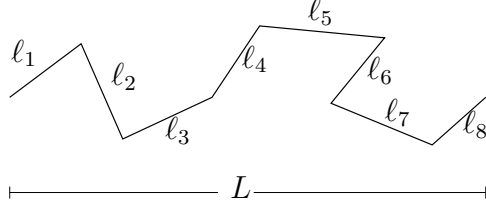


**Figure 15:** The small segments form a typical path traveled by an element of fluid in a porous medium.

a time interval  $(t_1, t_2)$ , which is  $\int_{t_1}^{t_2} \|\mathbf{x}'_f(t)\| dt$ , will be larger than the distance from  $\mathbf{x}_f(t_1)$  to  $\mathbf{x}_f(t_2)$ , i.e.

$$\frac{\int_{t_1}^{t_2} \|\mathbf{x}'_f(t)\| dt}{\|\mathbf{x}_f(t_2) - \mathbf{x}_f(t_1)\|} > 1. \quad (19)$$

Without being completely rigorous, we refer to the average value of the square of the above ratio over all fluid elements and time intervals  $(t_1, t_2)$ , as the tortuosity. We denote the tortuosity by  $\tau$ . This concept is illustrated in figure 15. If a typical path traveled by an element of fluid in a porous medium is through the segments with length  $\ell_i$  ( $1 \leq i \leq 8$ ), and the distance from the initial to the final positions of the element of fluid is  $L$ , then the tortuosity  $\tau$  is  $\tau = L^{-2}(\sum_{1 \leq i \leq 8} \ell_i)^2$ .

### 3.1.4 Relationship between the microscopic speed, the average velocity and the tortuosity

Let  $\mathbf{v}$  be what we have called the macroscopic fluid velocity, i.e.  $\mathbf{v}$  is the average of the fluid velocity in regions much larger than the pores but much smaller than the material. As before, let  $\mathbf{x}_f(t)$  be the path of an element of fluid. Note that, in fact,  $\mathbf{v}$  is the average of  $(t_2 - t_1)^{-1}(\mathbf{x}_f(t_2) - \mathbf{x}_f(t_1))$  over all fluid elements and time intervals  $(t_1, t_2)$  such that the distance between  $\mathbf{x}_f(t_1)$  and  $\mathbf{x}_f(t_2)$  is much larger than the typical pore linear dimension but much smaller than the material.

On the other hand, let  $v^*$  be the average fluid speed, i.e.  $v^*$  is the average of  $(t_2 - t_1)^{-1} \int_{t_1}^{t_2} \|\mathbf{x}'_f(t)\| dt$  over all fluid elements and time intervals  $(t_1, t_2)$ . It is clear, from the definition of tortuosity  $\tau$ , that

$$v^* = \sqrt{\tau} v \quad \text{where} \quad v = \|\mathbf{v}\|. \quad (20)$$

In other words, the ratio between the average of the microscopic fluid speed and the norm of the macroscopic fluid velocity is the tortuosity.

Analogously, we denote by  $\mathbf{u}$  be the macroscopic fines velocity, i.e.  $\mathbf{u}$  is the average of the velocities of the fines in regions much larger than the pores but much smaller than the material size, and by  $u^*$  the the average speed of the fines. We also have that

$$u^* = \sqrt{\tau}u \quad \text{where} \quad u = \|\mathbf{u}\|. \quad (21)$$

Note that these velocities and speeds are in general functions of the spatial position  $\mathbf{x}$  and time  $t$ , i.e.  $\mathbf{v} = \mathbf{v}(\mathbf{x}, t)$ ,  $\mathbf{u} = \mathbf{u}(\mathbf{x}, t)$ ,  $v^* = v^*(\mathbf{x}, t)$  and  $u^* = u^*(\mathbf{x}, t)$ .

### 3.1.5 Macroscopic fines velocity as function of the macroscopic fluid velocity

Our goal is to find  $\mathbf{u}$  as a function of  $\mathbf{v}$ . We will assume, naturally, that  $\mathbf{u}$  has the same direction as  $\mathbf{v}$ . Note that equation (18) provides a relationship between the speeds  $u^*$  and  $v^*$ , where  $L$  should be taken as a typical pore size. Thus, given equations (20) and (21) we have

$$1 = \frac{v}{\alpha} \left[ \frac{\alpha}{u} - \left(1 - e^{-\frac{\alpha}{u}}\right) \right] \quad \text{where} \quad \alpha = \frac{\kappa L}{\sqrt{\tau}} = \frac{9}{2} \frac{\mu L}{\sqrt{\tau} \rho_p r_p^2}, \quad (22)$$

and as before,  $v = \|\mathbf{v}\|$  and  $u = \|\mathbf{u}\|$ . The above equation is the key result of this section and will be used in the macroscopic model of next section.

### 3.1.6 Behavior of the macroscopic fines velocity vs. macroscopic fluid velocity curve

Let  $f(s) = s - (1 - e^{-s})$ . Note that equation (22) can be written as  $\alpha/v = f(\alpha/u)$ . From this simple observation we can draw some conclusions. Since  $f(0) = 0$ ,  $0 < f'(s) < 1$  for all  $s > 0$  and  $\lim_{s \rightarrow \infty} f(s) = \infty$  then

1.  $0 < u < v$  for all  $v > 0$  and for each  $v$  there exists a unique corresponding  $u$ .

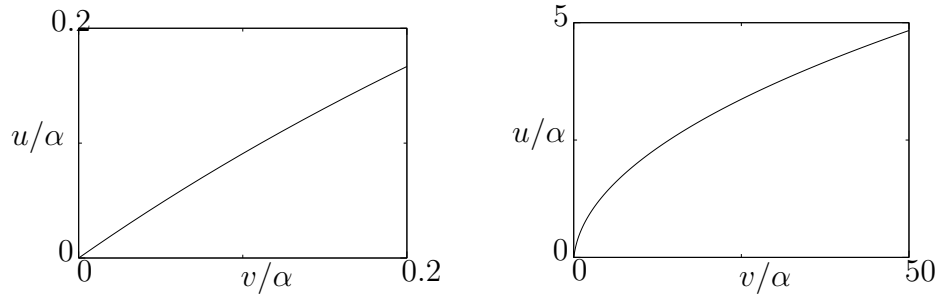


**Figure 16:** Plot of  $v/\alpha$  vs.  $u/\alpha$ . Both plots correspond to the same curve. They are just in different scales.

2.  $u$  is an increasing function of  $v$ .

The asymptotic behavior of  $u$  for both small and large values of  $v$  is also straight forward to obtain:

$$u \approx v \quad \text{for } v \ll \alpha, \quad (23)$$

and

$$u \approx \sqrt{\frac{\alpha v}{2}} \quad \text{for } v \gg \alpha. \quad (24)$$

A plot of  $v/\alpha$  vs.  $u/\alpha$  is shown in figure 16.

## 3.2 Evolution equation for the concentration of fines and clogging criteria

### 3.2.1 Porosity

Assume that our two-dimensional porous medium occupies the region  $\Omega$  and that  $\mathbf{x} \in \Omega$ .

We will denote by  $\phi = \phi(\mathbf{x})$  the porosity, i.e. the local volume fraction of void or pore space. More precisely, let  $B_\delta$  be the ball or radius  $\delta$  centered at  $\mathbf{x}$ . Let  $V_\delta$  be the void volume within  $B_\delta$  (really, the void area since we are considering two-dimensional materials). Let  $|B_\delta|$  be the volume of  $B_\delta$ . Then,  $\phi(\mathbf{x})$  is the asymptotic value of  $V_\delta/|B_\delta|$  for  $\delta$  much smaller than the material size but much bigger than the pore size

$$\phi(\mathbf{x}) = \frac{\text{void volume in } \{\mathbf{y} : \|\mathbf{y} - \mathbf{x}\| < \delta\}}{\text{volume of } \{\mathbf{y} : \|\mathbf{y} - \mathbf{x}\| < \delta\}}. \quad (25)$$

Note that  $\phi = \phi(\mathbf{x})$  may depend on  $\mathbf{x}$  but is independent of  $t$ .

### 3.2.2 Volume fraction of fines and volume fraction of fluid

We will denote by  $z = z(\mathbf{x}, t)$  the volume fraction of fines. More precisely,  $z(\mathbf{x}, t)$  is the asymptotic value of the volume of fines in  $B_\delta$  divided by volume of  $B_\delta$  for  $\delta$  much smaller than the material size but much bigger than the pore size

$$z(\mathbf{x}, t) = \frac{\text{volume of fines in } \{\mathbf{y} : \|\mathbf{y} - \mathbf{x}\| < \delta\}}{\text{volume of } \{\mathbf{y} : \|\mathbf{y} - \mathbf{x}\| < \delta\}}. \quad (26)$$

Note that  $z(\mathbf{x}, t)$  may depend on both  $\mathbf{x}$  and  $t$ . Note also that the volume fraction of fluid is  $\phi(x) - z(\mathbf{x}, t)$ . We will refer to  $z$  as the concentration of fines.

### 3.2.3 Fluid flow

Note also that, macroscopically, i.e. in a scale much bigger than the pore size and much smaller than the material size, fluid is convected with what we have called the macroscopic fluid velocity  $\mathbf{v}$  and the concentration of fines is convected with the macroscopic fines velocity  $\mathbf{u}$ . Since we assume that both particles and fluid are incompressible, the equation of mass conservation reduces to

$$\nabla \cdot (\mathbf{v}(\phi - z) + \mathbf{u}z) = 0, \quad (27)$$

where  $\nabla \cdot$  is the divergence operator.

In the small concentration of fines limit, i.e.  $z \ll \phi$ , and when  $\phi$  is independent of  $\mathbf{x}$ , equation (27) reduces to

$$\nabla \cdot \mathbf{v} = 0. \quad (28)$$

According to the discussions in the introduction, i.e. our motivation to study the plugging of media near well and given circular geometry of wells, we assume our material to occupy the region of the plane  $\{R_\ell \leq \|\mathbf{x}\|\}$ , where  $R_\ell$  is a constant. We will also assume that fluid flows at a known constant rate and with circular symmetry

toward the inner boundary  $\{\|\mathbf{x}\| = R_\ell\}$ . Thus, introducing the radial variable

$$r = \|\mathbf{x}\|, \quad (29)$$

we have that the velocity  $\mathbf{v}$  is of the form

$$\mathbf{v} = -v \frac{\mathbf{x}}{r} \quad \text{with} \quad v = \frac{A}{r}, \quad (30)$$

where  $A$  is a known positive constant. Note that  $2\pi A$  is the rate at which fluid exits the medium through the inner boundary.

### 3.2.4 Macroscopic fines velocity as function of $r$

The macroscopic fines velocity will also have a similar form as the macroscopic fluid velocity  $\mathbf{v}$ , i.e.

$$\mathbf{u} = -u \frac{\mathbf{x}}{r} \quad (31)$$

where  $u$  and  $v$  are related by equation (22) and thus,  $u = u(r)$ . Since we now have  $v$  in terms of  $r$  (equation (30)), we can now combine equations (22) and (30) to obtain a relation between  $u$  and  $r$ , namely

$$\frac{\alpha r}{A} = \frac{\alpha}{u} - (1 - e^{-\frac{\alpha}{u}}), \quad (32)$$

where  $\alpha$  was defined in equation (22). Note that, from the results of subsection 3.1.6 and equation (30) we have that  $u$  is a decreasing function of  $r$ .

The asymptotic behavior of  $u$  for both small and large values of  $r$  is also straight forward to obtain:

$$u \approx \frac{A}{r} \quad \text{for} \quad r \gg \frac{A}{\alpha}, \quad (33)$$

and

$$u \approx \sqrt{\frac{\alpha A}{2r}} \quad \text{for} \quad r \ll \frac{A}{\alpha}. \quad (34)$$

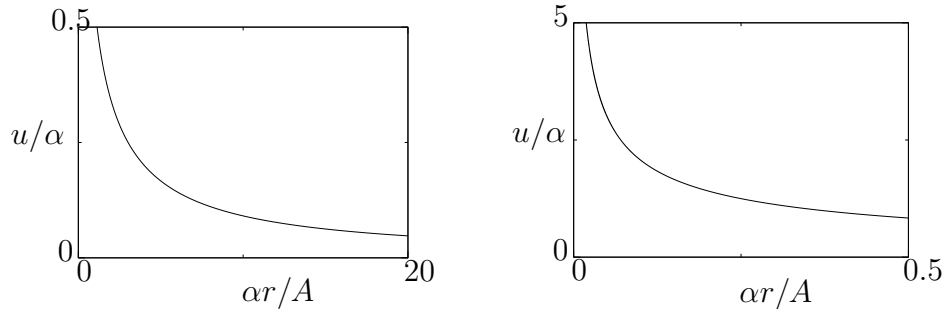


**Figure 17:** Plot of  $\alpha r/A$  vs.  $u/\alpha$ . Both plots correspond to the same curve. They are just in different scales.

A plot of  $\alpha r/A$  vs.  $u/\alpha$  is shown in figure 17.

Note that the difference between the fluid and fines macroscopic velocities are more pronounced for small values of  $r$ .  $v$  increases proportionally to  $r^{-1}$  as  $r \rightarrow 0$ , but  $u$  increases proportionally to  $r^{-1/2}$ .

### 3.2.5 Transport of fines

Since  $z$ , the concentration of fines, is convected with the macroscopic fines velocity  $\mathbf{u}$ , we have the following conservation equation

$$\frac{\partial z}{\partial t} + \nabla \cdot (\mathbf{u}z) = 0. \quad (35)$$

Note that we neglect dispersion. Given the circular symmetry of our problem and equation (31), and assuming circular symmetry also in the initial conditions for  $z$ , the above equation reduces to

$$\frac{\partial z}{\partial t} - \frac{1}{r} \frac{\partial(ruz)}{\partial r} = 0, \quad (36)$$

where  $u = u(r)$  is a function of  $r$  given implicitly in equation (32).

We remark that the dependence of  $u = u(r)$  as a function of  $r$  was obtained under the assumption that  $z$  is small, i.e.  $z \ll \phi$ . Nevertheless, we will use equation (32) even when the restriction  $z \ll \phi$  is not satisfied. The reason being that using equation (32) adds clarity to our exposition while keeping the physical effects we are interested in modeling in this work.

Note that the evolution of the concentration of fines  $z(r, t)$  is completely determined by equations (32) and (36) once the initial conditions are given, i.e. we need to know  $z(r, 0)$ .

### ***3.3 Fines accumulate as they are convected toward the inner boundary***

Note that the evolution equation for the concentration of fines  $z$  is hyperbolic and can be solved by the method of characteristics. More precisely, we first write equation (36) as

$$\frac{\partial z}{\partial t} - u \frac{\partial z}{\partial r} = \frac{1}{r} \frac{d(ru)}{dr} z. \quad (37)$$

For convenience we define

$$\sigma = \sigma(r) = \frac{1}{r} \frac{d(ru)}{dr}. \quad (38)$$

In characteristic form, the equation (37) reads

$$\begin{aligned} \bar{r}'(t) &= -u(\bar{r}(t), t) \\ \frac{dz}{dt}(\bar{r}(t), t) &= \sigma(\bar{r}(t))z(\bar{r}(t), t), \end{aligned} \quad (39)$$

where  $\bar{r}'$  is the derivative of  $\bar{r}$  with respect to  $t$ .

As a first observation, we show in the appendix A.1 that  $\sigma$  is always positive. Thus, the concentration of fines  $z$  is always increasing along the characteristic paths, i.e.  $z(\bar{r}(t), t)$  is an increasing function of time. In other words, fines accumulate as they are convected toward the inner boundary.

As a second observation, note that the equation (37) is linear and thus, characteristics do not cross. In particular, we do not have formation of shocks.

In figure 18 we show an example of the time evolution of  $z$ . We plotted  $r/R_\ell$  vs.  $z$  for four fixed values of  $t$ :  $t = 0$ ,  $t = R_\ell/\alpha$ ,  $t = 5R_\ell/\alpha$  and  $t = 100R_\ell/\alpha$ . The initial condition was  $z(r, 0) = 0.1$ . Note that  $z(r, t)$  is defined only for  $r \geq R_\ell$ .

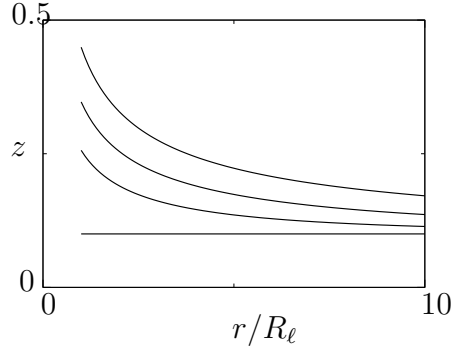


**Figure 18:** Plot  $r/R_\ell$  vs.  $z$  for four fixed values of  $t$ :  $t = 0$ ,  $t = R_\ell/\alpha$ ,  $t = 5R_\ell/\alpha$  and  $t = 100R_\ell/\alpha$ .  $z$  increases with  $t$ .

The necessary calculations were computed numerically. Note that  $z(r, t)$  approaches a bounded value as  $t \rightarrow \infty$  for all  $r$ . The profile of  $z$  as  $t \rightarrow \infty$  is similar to the profile for  $t = 100R_\ell/\alpha$ . As expected,  $z$  increases with  $t$ .

### 3.4 *Criterion for clogging*

As previewed in the introduction, our criterion for clogging is very simple. Regions of the medium plug if and when the concentrations of fines  $z$  in those regions exceed a certain critical value  $z_*$ . Note that, given the symmetry of our system, the region that plugs first is a ring centered at  $r = 0$ . Once this ring is plugged, there is no more flow through the medium. As we will study in later sections, clogging may or may not occur. The outcome will depend on the parameters of the system.

### 3.5 *Homogeneous initial conditions*

In this section we will study the evolution of concentration of fines  $z$  assuming that initially the concentration of fines is homogeneous, i.e.

$$z(r, 0) = z_0 \quad \text{for all } r \geq R_\ell. \quad (40)$$

where  $z_0$  is a known positive constant.

#### 3.5.1 *The concentration of fines is a decreasing function of $r$*

A key observation is the following

**Observation 3.5.1.**  $z(r, t)$  is a decreasing function of  $r$  for any fixed  $t$ .

*Proof.* Let  $t$  be fixed. Let  $r_1 < r_2$ . Let  $\bar{r}_1(s)$  be the characteristic, i.e. a solution of the system (39), that satisfies  $\bar{r}_1(t) = r_1$ . Let  $\bar{r}_2(s)$  be the characteristic that satisfies  $\bar{r}_2(t) = r_2$ . Since characteristics do not cross, we necessarily have  $\bar{r}_1(s) < \bar{r}_2(s)$  for all  $0 \leq s \leq t$ . Note that equation (39) implies that

$$z(r_1, t) = z_0 e^{\int_0^t \sigma(\bar{r}_1(s)) ds} \quad \text{and} \quad z(r_2, t) = z_0 e^{\int_0^t \sigma(\bar{r}_2(s)) ds}. \quad (41)$$

Since, as shown in the appendix A.3,  $\sigma(r)$  is a decreasing function of  $r$ , we conclude that  $z(r_1, t) > z(r_2, t)$  for all  $r_1 < r_2$  and  $t > 0$ , which concludes the proof of this observation.  $\square$

### 3.5.2 Clogging may only occur at the inner boundary

Observation 3.5.1 implies that, if  $z$  reaches the critical value  $z_*$ , it will first reach that value at  $r = R_\ell$ . Thus, we have the following observation

**Observation 3.5.2.** *If the medium plugs, the region that clogs is the ring  $r = R_\ell$ .*

### 3.5.3 Determining if clogging does occur

Consider one fixed characteristic  $\bar{r}(t)$ , i.e.  $\bar{r}(t)$  is a solution of the system (39). Let  $\bar{z}(t) = z(\bar{r}(t), t)$  and  $\bar{u}(t) = u(\bar{r}(t))$ . Note that  $\bar{r}(t)$  is a strictly decreasing function of  $t$  and  $u(r)$  is a strictly decreasing function of  $r$ . Thus,  $\bar{u}(t)$  is a strictly increasing function of  $t$  and we can regard  $t$  as a function of  $\bar{u}$ . Thus,  $\bar{z}$  can also be regarded as a function of  $\bar{u}$ . In the appendix A.4 we compute  $d\bar{z}/d\bar{u}$ . More precisely, defining the function

$$G(s) = \frac{1}{s} \left[ \frac{1}{s} - \left( 1 - e^{-\frac{1}{s}} \right) \right]^{-1} \left[ 1 - \left( 1 + \frac{1}{s} \right) e^{-\frac{1}{s}} \right], \quad (42)$$

we show that

$$\frac{d\bar{z}}{d\bar{u}} = \frac{1}{\alpha} G\left(\frac{\bar{u}}{\alpha}\right) \bar{z}. \quad (43)$$

Note that  $G(s) > 0$  for all  $s > 0$ .

We now compute the value of  $\bar{z}$  at the time the characteristic  $\bar{r}$  reaches the inner boundary, i.e.  $\bar{r} = R_\ell$ . This value will depend on the initial location of the characteristic, i.e.  $\bar{r}_0 = \bar{r}(0)$ . Let  $u_0$  be the macroscopic fines velocity at  $r = \bar{r}_0$ , i.e.  $u_0$  is the solution of equation (32) when  $r = \bar{r}_0$ . Let  $u_\ell$  be the macroscopic fines velocity at the inner boundary,  $r = R_\ell$ . Clearly  $u_\ell > u_0$ . We denote by  $\bar{z}_\ell$  the value of  $\bar{z}$  at the inner boundary. Given equation (43) and noticing that  $\bar{z}$  should be equal to  $z_0$  when  $\bar{u} = u_0$  because that corresponds to the initial location of the characteristic, we have that  $\bar{z}$  at the inner boundary is

$$\bar{z}_\ell = z_0 \exp \left( \int_{u_0}^{u_\ell} \frac{1}{\alpha} G \left( \frac{\bar{u}}{\alpha} \right) d\bar{u} \right). \quad (44)$$

Note that

$$\frac{d}{ds} \ln \left[ 1 - s \left( 1 - e^{-\frac{1}{s}} \right) \right] = -G(s). \quad (45)$$

Thus,

$$\bar{z}_\ell = z_0 \left[ \frac{1 - \frac{u_0}{\alpha} \left( 1 - e^{-\frac{\alpha}{u_0}} \right)}{1 - \frac{u_\ell}{\alpha} \left( 1 - e^{-\frac{\alpha}{u_\ell}} \right)} \right]. \quad (46)$$

Note that the furthest from the inner boundary the characteristic started, the largest the value of the concentration when it reaches the boundary. This is clear from intuition and it can also be seen directly in equation (44). The furthest from the inner boundary the characteristic started, the smallest the value of  $u_0$  and the largest the value of  $\bar{z}_\ell$ . The limit of infinitely farthest corresponds to an initial macroscopic fines velocity of 0, i.e.  $u_0 = 0$ . Thus, there will be clogging if and only if  $\bar{z}_\ell > z_\star$  when  $u_0 = 0$ .

We summarize our finding in the following observation. For convenience in the computations, we state the observation in dimensionless form. More precisely, in the below observation,  $s_\ell = u_\ell/\alpha$ , where  $u_\ell$  is the macroscopic fines velocity at the inner

boundary  $r = R_\ell$ , and the left hand side of equation (48) is  $\lim_{t \rightarrow \infty} z(R_\ell, t)/z_0$ , the limit of the concentration of fines at  $r = R_\ell$  divided by  $z_0$  as  $t \rightarrow \infty$  or, equivalently, the left hand side of equation (48) is the value of  $z/z_0$  in the limit when the characteristic that starts infinitely far reaches the inner boundary.

**Observation 3.5.3.** *Let  $s_\ell$  be the root of*

$$\frac{\alpha R_\ell}{A} = \frac{1}{s_\ell} - \left(1 - e^{-\frac{1}{s_\ell}}\right). \quad (47)$$

*The medium plugs if and only if*

$$\frac{1}{1 - s_\ell \left(1 - e^{-\frac{1}{s_\ell}}\right)} > \frac{z_\star}{z_0}. \quad (48)$$

### 3.5.4 The parameter regime where the medium plugs

As it is clear from observation 3.5.3, whether the medium plugs or not depends on the relationship between two dimensionless parameters,  $A/(\alpha R_\ell)$  and  $z_\star/z_0$ . More precisely, we state observation 3.5.3 in an equivalent form that is more convenient to plot in the parameter plane  $z_\star/z_0$  vs.  $A/(\alpha R_\ell)$ .

**Observation 3.5.4.** *Let  $s_c$  be the unique solution of*

$$\frac{1}{1 - s_c \left(1 - e^{-\frac{1}{s_c}}\right)} = \frac{z_\star}{z_0}. \quad (49)$$

*Then, the medium plugs if and only if*

$$\frac{A}{\alpha R_\ell} \geq \frac{s_c}{1 - s_c \left(1 - e^{-\frac{1}{s_c}}\right)}. \quad (50)$$

In figure 19 we display the regions in the parameter plane  $z_\star/z_0$  vs.  $A/(\alpha R_\ell)$  where clogging does and does not occur.

The parameter  $z_\star/z_0$  indicates how many times the concentration of fines needs to increase for the medium to plug. Note that  $A/R_\ell$  is the macroscopic fluid velocity  $v$  at the inner boundary and  $\alpha$ , defined in equation (22), is a velocity that depends

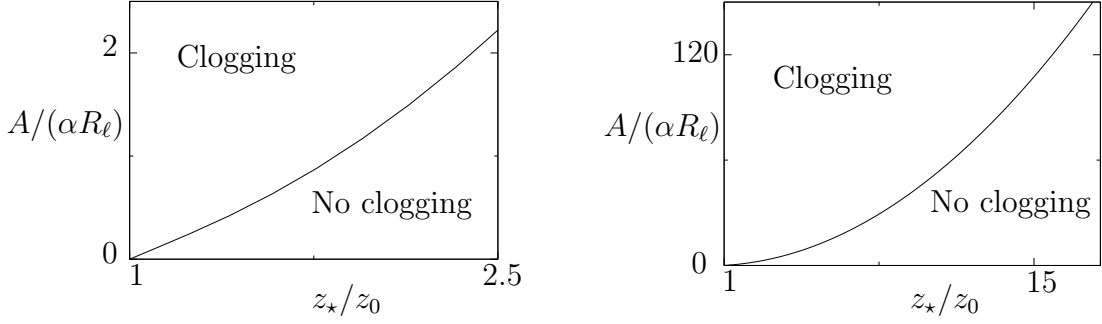


**Figure 19:** Regions in the parameter plane  $z_*/z_0$  vs.  $A/(\alpha R_\ell)$  where clogging does and does not occur. Both plots correspond to the same regions. They are just in different scales.

on microscopic parameters of the system. Note that  $\alpha$  indicates when the difference between the macroscopic fluid velocity  $v$  and macroscopic fines velocity  $u$  is noticeable. More precisely,  $u \approx v$  if and only if  $v \ll \alpha$ .

The asymptotic form of the curve in figure 19, that divides the parameter region where the medium does and does not plug, can be easily obtained when  $(z_*/z_0 - 1) \ll 1$  and  $z_*/z_0 \gg 1$ . These calculations are done in the appendix A.5. Here we summarize our findings in the following observation.

**Observation 3.5.5.** *The boundary in the parameter plane  $z_*/z_0$  vs.  $A/(\alpha R_\ell)$  between the regions where the medium plugs and does not plug satisfies the following asymptotic behaviors*

$$\frac{A}{\alpha R_\ell} \approx \frac{z_*}{z_0} - 1 \quad \text{if } \frac{z_*}{z_0} - 1 \ll 1 \quad (51)$$

and

$$\frac{A}{\alpha R_\ell} \approx \frac{1}{2} \left( \frac{z_*}{z_0} \right)^2 \quad \text{if } \frac{z_*}{z_0} \gg 1. \quad (52)$$

### 3.5.5 Avoiding clogging

Our work is motivated by the plugging of media around wells that is sometimes observed. Once this occurs, no more petroleum or water can be extracted from the well. Clearly, this is an undesirable effect. On one hand, it is tempting to increase the

pumping rate to maximize gains. However, our model implies that, if this pumping rate is large enough, the medium will plug. Our analysis shows the maximum rate at which fluid can be extracted without plugging the medium. First we have to estimate the parameters  $z_*$ ,  $z_0$  and  $\alpha$ . The maximum macroscopic fluid velocity at the well to avoid clogging is  $A/R_\ell$ , solution of the system (49) and (50). Of course, our model is the result of simplifications in the attempt to isolate physical effects that we believe have a dominant contribution in the plugging of media around well. Thus, our works should be regarded as guidelines to motivate the development of more quantitative precise models and related laboratory and field experiments. It should not be regarded as a model that will match experiments quantitatively with large precision.

### 3.5.6 Clogging time when clogging does occur

We now assume that clogging does occur and our goal is to compute the time  $t = t_c$  it takes the material to plug.

Let  $\bar{r}(t)$  be the characteristic where clogging occurs. Thus,  $\bar{r}(t_c) = R_\ell$ . We define  $\bar{z}(t) = z(\bar{r}(t), t)$  and  $\bar{u}(t) = u(\bar{r}(t))$ . Note that  $\bar{z}(t_c) = z_*$  and  $\bar{u}(t_c) = u_\ell = u(R_\ell)$ , the macroscopic fines velocity at the inner boundary. Also note that, it follows from equation (32), that  $u_\ell$  is solution of

$$\frac{\alpha R_\ell}{A} = \frac{\alpha}{u_\ell} - \left(1 - e^{-\frac{\alpha}{u_\ell}}\right). \quad (53)$$

Our first step in computing the clogging time  $t_c$  is to obtain  $u_\ell$  from the last equation.

Let  $u_0 = u(\bar{r}(0))$ , i.e.  $u_0$  is the macroscopic fines velocity in the characteristic  $\bar{r}$  at time equal  $t = 0$ . Equation (46) and the above observations imply that

$$z_* = z_0 \left[ \frac{1 - \frac{u_0}{\alpha} \left(1 - e^{-\frac{\alpha}{u_0}}\right)}{1 - \frac{u_\ell}{\alpha} \left(1 - e^{-\frac{\alpha}{u_\ell}}\right)} \right]. \quad (54)$$

From the last equation we can obtain  $u_0$  after  $u_\ell$  is obtained from equation (54).

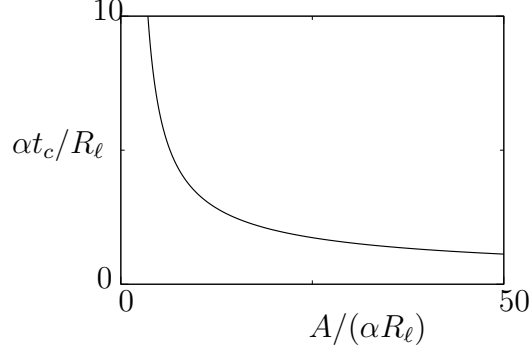


**Figure 20:**  $A/(\alpha R_\ell)$  vs.  $\alpha t_c/R_\ell$  where  $z_*/z_0 = 2$ .

As argued previously, we can regard  $t$  as function of  $\bar{u}$ . In the appendix A.6 we show that

$$\frac{dt}{d\bar{u}} = \frac{A}{\bar{u}^3} (1 - e^{-\frac{\alpha}{\bar{u}}}). \quad (55)$$

We can integrate the above equation noticing that  $\bar{u} = u_0$  when  $t = 0$  and  $\bar{u} = u_\ell$  when  $t = t_c$  to obtain

$$\frac{\alpha^2 t_c}{A} = \left( \frac{1}{2} \frac{\alpha^2}{u_0^2} + \left(1 + \frac{\alpha}{u_0}\right) e^{-\frac{\alpha}{u_0}} \right) - \left( \frac{1}{2} \frac{\alpha^2}{u_\ell^2} + \left(1 + \frac{\alpha}{u_\ell}\right) e^{-\frac{\alpha}{u_\ell}} \right). \quad (56)$$

Once  $u_0$  and  $u_\ell$  are obtained from equations (54) and (55),  $t_c$  can be obtained from the equation (56).

In figure 20 we show a plot of  $A/(\alpha R_\ell)$  vs.  $\alpha t_c/R_\ell$ . As expected, the clogging time  $t_c$  decreases with the flow rate  $2\pi A$ . In particular, we show in the appendix A.7 that the clogging time  $t_c$  decays like  $-1/2$  power of the flow rate. More precisely, we find that

$$\frac{\alpha t_c}{R_\ell} = \frac{\sqrt{8}}{3} \left[ \left( \frac{z_*}{z_0} \right)^3 - 1 \right] \sqrt{\frac{\alpha R_\ell}{A}} \quad \text{if } \frac{A}{\alpha R_\ell} \gg 1. \quad (57)$$

### 3.5.7 Volume of fluid extracted before the medium plugs

If clogging does occur, a quantity of interest is the volume (area in our two-dimensional problem) of fluid  $V_f$  that exits the medium through the inner boundary before clogging

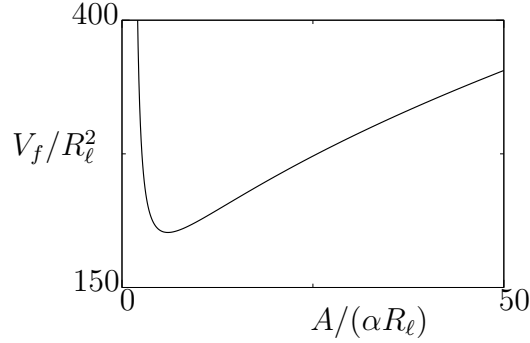


**Figure 21:**  $A/(\alpha R_\ell)$  vs.  $V_f/R_\ell^2$  where  $z_\star/z_0 = 2$ .

occurs. In the case of wells, this is the volume of fluid extracted before the medium plugs and the well is no longer of use. Note that, if the medium plugs at  $t = t_c$ , the volume of fluid  $V_f$  that exits the medium through the inner boundary before clogging occurs is

$$V_f = 2\pi A t_c. \quad (58)$$

In figure 21 we show a plot of  $A/(\alpha R_\ell)$  vs.  $V_f/R_\ell^2$ .

The clogging time  $t_c$  becomes unbounded as we approach from above the critical flow rate at which there is no more clogging for smaller rates. Thus, as expected, the volume extracted also becomes unbounded in this limit. On the other hand, from equation (57), we have that

$$\frac{V_f}{R_\ell^2} = \frac{\sqrt{8}}{3} \left[ \left( \frac{z_\star}{z_0} \right)^3 - 1 \right] \sqrt{\frac{A}{\alpha R_\ell}} \quad \text{if } \frac{A}{\alpha R_\ell} \gg 1. \quad (59)$$

Thus, even though the clogging time  $t_c$  tends to 0 as the flow rate  $2\pi A$  increases,  $V_f$  does not. In fact,  $V_f \rightarrow \infty$  in this limit. The reason being is that  $t_c$  decreases like a  $-1/2$  power of  $A$  and thus,  $V_f = 2\pi A t_c$  increases like a  $1/2$  power of  $A$ . As illustrated in figure 21,  $V_f$  has a unique local minimum that is also the global minimum that occurs at some finite value of  $A$ .

### ***3.6 Conclusions***

In this chapter, we have introduced a multi-scale model that captures and isolates the role of inertia of the particles and tortousity of the fluid paths in the plugging of porous media near wells, where the macroscopic fluid velocity is non-homogeneous. We refer to our model as a multi-scale model because it resulted from first developing a model at the pore-scale and then using the result of this model as input of a macro-scale model. While simple, the model obtained captures the physics we pursued to study. Our model has proved amenable to analysis and computations. In particular, we were able to identify dimensionless parameters that, according to our model, determine whether the medium plugs. We were also able to make detailed parameter studies. We believe this chapter will serve as a step toward more comprehensive modeling of plugging of porous media and it will serve to guide laboratory and field experiments to shed more light into the physics involved in the complex and important phenomenon of plugging of porous media.

## CHAPTER IV

### THE EFFECT OF THE MICRO-GEOMETRY ON THE PERFORMANCE OF FILTERS

As previewed in the introduction, in this chapter we study particle migration and clogging as suspension flows through filters by means of numerical simulations and elementary analysis. We model filters as networks of channels. Each channel is either open or clogged. There is no flow through clogged channels. Each particle and each channel is assigned a width. Particles flow with the fluid while inside a wider channel. When reaching an intersection of channels, a particle flows into a new channel. If this new channel is thinner than the particle, the particle is trapped and the channel clogged.

The geometries of the networks we study in this chapter are regular: one-dimensional network and two-dimensional square and hexagonal networks. We study the case when the width of the channels and of the particles are independent random variables. We select a probability distribution for the width of the channels and a second one for the width of the particles. Among other questions, in this chapter we do a series of studies that seek to answer the following questions in terms of the geometry of the network, the probability distribution of the width of the channels and the probability distribution of the width of the particles:

1. What is the proportion of particles that are trapped?
2. What is the proportion of channels clogged when the filter ceases to be effective?
3. How does the filter permeability decreases during its life time?

We also study some deterministic filters, i.e. the width of the channels and particles

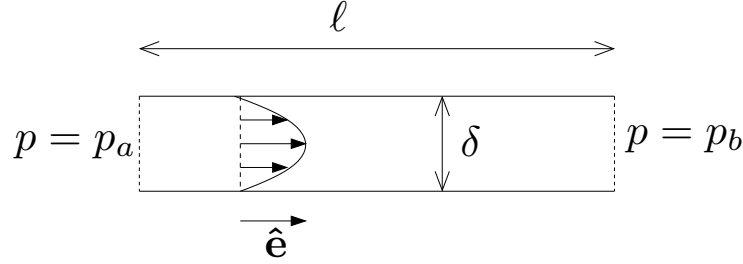


**Figure 22:** Velocity profile of a Poiseuille flow within a straight channel (indicated by arrows).

are not random, that are optimal in some sense.

## 4.1 Mathematical model

### 4.1.1 Fluid flow in channels

Figure 22 shows a two-dimensional channel with length  $\ell$  and width  $\delta$  filled with a Newtonian incompressible fluid that is subjected to pressures  $p = p_a$  and  $p = p_b$  at the ends of the channel. Let  $\hat{e}$  be the vector of unit length parallel to the channel displayed in figure 22. Let  $y$  be the coordinate in the direction perpendicular to the channel. At low Reynolds numbers (low velocities), the fluid velocity of the steady state flow is of the form  $u(y)\hat{e}$  with  $u$  satisfying  $(p_b - p_a)/\ell = \mu u''$ , where  $\mu$  is the fluid viscosity and  $u''$  is the second derivative of  $u$ . In addition, the fluid velocity satisfies no slip boundary conditions at the channel walls, i.e.  $u = 0$  at the walls. Simple calculations show that the velocity has a parabolic profile (see figure 22) and its spatial average across the channel is (see [2])

$$\mathbf{v} = K_e(p_a - p_b)\hat{e} \quad \text{where } K_e = \frac{\delta^2}{12\mu\ell}. \quad (60)$$

This type of flow is known as Poiseuille flow.

### 4.1.2 Filter geometry

We model filters as two-dimensional networks of channels as we illustrate in figure 23. The voids are the interior of the channels. Our filters have a bottom boundary at

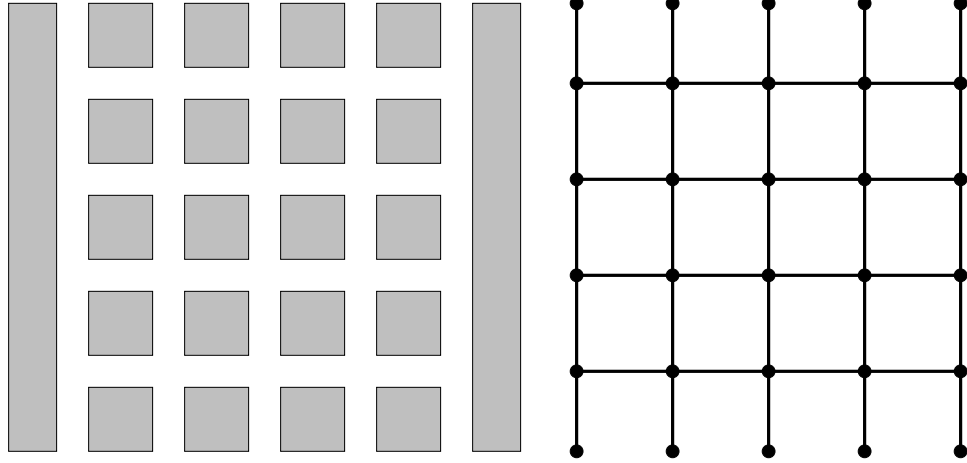


**Figure 23:** Example of a network of one of our filters and the corresponding graph.

$y = y_b$  and a top boundary at  $y = y_t$ . To each filter we associate a graph in a natural way. The edges are the channels and the nodes the end points of the edges, see figure 22. Note that the graph is included in  $y_b \leq y \leq y_t$ . Note that there are nodes in the bottom and top boundaries but no edge is included in the bottom or top boundary. We denote by  $\mathcal{N}$  the set of nodes. We identify the nodes with their location and thus,  $\mathcal{N} \subset \mathbb{R}^2$ . We denote by  $\mathcal{E}$  the set of edges. Given an edge  $e$ , its width (i.e. the width of the channel that corresponds to  $e$ ) is denoted by  $\delta_e$  and its length by  $\ell_e$ . We assume that the widths of the channels are much smaller than their lengths.

### 4.1.3 Fluid flow in networks

The particles within the network are incompressible. The fluid is incompressible Newtonian fluid with constant density  $\rho$  and constant viscosity  $\mu$  and satisfies non-slip boundary conditions, i.e. the fluid velocity vanishes at the channels walls.

For each node  $\mathbf{a} \in \mathcal{N}$ , we denote by  $p_{\mathbf{a}}$  the pressure at  $\mathbf{a}$ . Note that  $p_{\mathbf{a}} = p_{\mathbf{a}}(t)$  is a function of time  $t$ . We assume that the bottom boundary is held at constant pressure  $p = p_b$  and the top boundary at  $p = p_t$ , where  $p_b > p_t$ . Thus, the pressures at the

nodes satisfy the boundary condition

$$p_{\mathbf{a}} = p_b \quad \text{if } \mathbf{a} \in \{y = y_b\} \quad (61)$$

$$p_{\mathbf{a}} = p_t \quad \text{if } \mathbf{a} \in \{y = y_t\}. \quad (62)$$

If  $e$  is an open edge, we denote by  $\mathbf{v}_e$  the average of the velocity field within the channel  $e$ .  $\mathbf{v}_e$  is proportional to the pressure drop across  $e$ . Thus, if  $\mathbf{a}$  and  $\mathbf{b}$  are the endpoints of  $e$ , then

$$\mathbf{v}_e = -K_e (p_{\mathbf{b}} - p_{\mathbf{a}}) \frac{\mathbf{b} - \mathbf{a}}{\|\mathbf{b} - \mathbf{a}\|}, \quad \text{if } e \text{ is open,} \quad (63)$$

where we use the standard notation for the euclidean norm  $\|\mathbf{r}\| = \sqrt{r_1^2 + r_2^2}$ . If the channel is straight, the constant  $K_e$  is as given in equation (60).

On the other hand, if  $e$  is clogged, there is no flow within  $e$ . Thus,

$$\mathbf{v}_e = 0 \quad \text{if } e \text{ is clogged.} \quad (64)$$

The rate at which volume of fluid enters an intersection is equal to the rate at which it leaves the intersection, i.e. conservation of mass. This implies that, for each node  $\mathbf{a}$ , we have

$$\sum_{\{e \in \mathcal{E}: \mathbf{a} \text{ is an endpoint of } e\}} \delta_e \mathbf{v}_e \cdot \frac{\mathbf{b} - \mathbf{a}}{\|\mathbf{b} - \mathbf{a}\|} = 0, \quad \text{where } \mathbf{b} \text{ is the endpoint of } e \text{ not equal to } \mathbf{a}. \quad (65)$$

The velocities within all the channels are uniquely determined by the system (61-65). This well known system (similar models were used as early as [15, 16, 17], see also [49, 13]) is the asymptotics of the Navier-Stokes equations within the void with non-slip boundary condition in the limit when the widths of the channels are much smaller than their lengths.

In practice, we first solve for the pressure at the nodes and then for the velocities within the channels. More precisely, using the expression for the velocities in equation (63), we reduce equation (65) into

$$\sum_{\{\mathbf{b} \in \mathcal{N}: \mathbf{b} \text{ is connected to } \mathbf{a} \text{ by an open edge}\}} \frac{\delta_e^3}{12\mu\ell_e} (p_{\mathbf{b}} - p_{\mathbf{a}}) = 0, \quad \text{for all } \mathbf{a} \in \mathcal{N}, \quad (66)$$

which together with the condition (61), reduce to a system of linear equations, where the number of unknowns is equal to the number of nodes in a single period cell minus one. Once the pressure at the nodes are obtained, the velocities in the open edges are easily computed with equation (63).

#### 4.1.4 Particle transport within the filter

Given an edge  $e$ , its endpoint with smallest pressure will be called its head and will be denoted by  $\mathbf{h}(e)$ . Analogously,  $\mathbf{k}(e)$ , the tail of the edge  $e$ , is the endpoint of  $e$  with largest pressure. Thus, fluid within an edge  $e$  (or channel) flows from its tail  $\mathbf{k}(e)$  to its head  $\mathbf{h}(e)$ . As we will proceed to explain, edges may change from open to clogged and vice versa. Thus, the fluid flow is time dependent and as a consequence, an endpoint of an edge may be its head for some period of time and its tail for other times.

Particles may enter the network at the bottom boundary only. The particles travel with the average fluid velocity within the edge they are in, i.e. if a particle is in the edge  $e$  at time  $t$ , the particle moves with velocity  $\mathbf{v}_e$  at time  $t$ .

Assume now that a particle reaches a node  $\mathbf{a}$  at time  $t$ . The particle will flow into a new edge. This new edge is selected as follows. Let  $e_1, \dots, e_r$  be the edges that have  $\mathbf{a}$  as tail, i.e.  $\mathbf{k}(e_i) = \mathbf{a}$  for  $1 \leq i \leq r$ . The edge the particle flows into is selected among  $e_1, \dots, e_r$  randomly. The probability of  $e_i$  being selected is proportional to the rate of flow into  $e_i$ , more explicitly

$$\text{probability particle flows into } e_i = \frac{\delta_{e_i} v_{e_i}}{\sum_{j=1}^r \delta_{e_j} v_{e_j}}. \quad (67)$$

If a particle enters an open edge  $e$  whose width  $\delta_e$  is smaller than or equal to the particle diameter, then the particle is trapped by the edge  $e$  and the status of  $e$  changes from open to clogged. For convenience we assume that the particle is actually trapped when it reaches the midpoint of  $e$ .

Our model allows particles to detach. Assume a particle was trapped in an edge

$e$  at time  $t = t_1$ . If at a later time  $t = t_2$ , the head and tail of  $e$  change end points, i.e.  $\mathbf{h}(e)(t_2) = \mathbf{k}(e)(t_1)$  and  $\mathbf{k}(e)(t_2) = \mathbf{h}(e)(t_1)$ , the particle is no longer trapped and starts moving and the edge becomes open again.

Note that, every time an edge clogs or opens the flow within the network changes.

#### 4.1.5 Channels and particles size

We assume the thickness of all the edges are independent random variables identically distributed. We denote by  $\delta$  a random variable with the same distribution as the thickness of any edge. Analogously, the diameter of all the particles are independent random variables identically distributed and we denote by  $d$  a random variable with the same distribution as the diameter of any particle. We will denote by  $f_d$  and  $f_\delta$  the probability distribution functions of  $d$  and  $\delta$  respectively. We use the standard notation of  $P(A)$  to denote the probability that the event  $A$  occurs. We recall that  $f$  is the probability distribution function of a random variable  $X$  if  $P(a \leq X \leq b) = \int_a^b f(x) dx$  for all numbers  $a \leq b$ . We allow the possibility of  $d$  or  $\delta$  not being continuous random variables in which case their probability distribution functions may be generalized functions, i.e. be a linear combination of a function with delta functions.

#### 4.2 *Probability that a particle is trapped in a clean filter*

In this section we will study the probability that one single particle is trapped by a filter in which all the edges are open. In particular, we will study the dependence of this probability on the height of the filter, i.e. the number of edges in the shortest path connecting the top with the bottom boundary. This section will provide us with intuition that will guide us in our more general studies of next section where we study our complete model.

### 4.2.1 One-dimensional filter

We start considering a one-dimensional filter. In other words, our filter is a path of edges connecting the bottom and top boundaries. More precisely, our filter has  $n + 1$  different nodes,  $\mathbf{a}_0, \mathbf{a}_1, \dots, \mathbf{a}_n$  and  $n$  edges,  $e_1, \dots, e_n$  such that the end points of  $e_i$  are  $\mathbf{a}_{i-1}$  and  $\mathbf{a}_i$ ,  $\mathbf{a}_0$  is a node in the bottom boundary,  $\mathbf{a}_n$  is a node in the top boundary and the other nodes do not belong to the top or bottom boundaries.

#### 4.2.1.1 General results

**Observation 4.2.1.** *The probability that the particle flows through all the edges without being trapped is*

$$P(\text{particles crosses the filter}) = \int_0^{+\infty} (P(\delta > x))^n f_d(x) dx \quad (68)$$

*Proof.* A particle flows through all the edges without being trapped if and only if its diameter is smaller than the diameter of all the edges. Thus,

$$P(\text{particle crosses the filter}) = \int_0^{+\infty} P\left(\min_{1 \leq i \leq n} \delta_{e_i} > x\right) f_d(x) dx. \quad (69)$$

Since the width of the edges are independent variables, we have

$$P\left(\min_{1 \leq i \leq n} \delta_{e_i} > x\right) = \prod_{i=1}^n P(\delta_{e_i} > x) = P(\delta > x)^n, \quad (70)$$

from where the validity of the observation follows.  $\square$

**Corollary 4.2.1.** *Whenever the diameter of a particle has the same distribution as the thickness of the edges, the probability that the particle flows through all the edges without being trapped is*

$$P(\text{particle crosses the filter}) = \frac{1}{n + 1}. \quad (71)$$

*Proof.* Note that  $f_d = f_\delta$  and thus,  $\frac{dP(\delta > x)}{dx}(x) = -f_\delta(x) = -f_d(x)$ . This allows us to compute the integral in the right hand side of equation (68)

$$\int_0^{+\infty} (P(\delta > x))^n f_d(x) dx = - \left[ \frac{(P(\delta > x))^{n+1}}{n + 1} \right]_0^{+\infty} = \frac{1}{n + 1}, \quad (72)$$

from which the results follows.  $\square$

**Observation 4.2.2.** *Assume that  $\delta$  and  $d$  are continuous random variables, i.e.  $f_\delta$  and  $f_d$  are classical functions. Assume  $\{f_d(x) > 0\} = (a, b)$  and  $\{f_\delta(x) > 0\} = (\alpha, \beta)$ , where  $b$  and  $\beta$  may be infinity. Assume that*

$$f_d(x) \approx K_d(x - a)^{\Lambda_d} \quad \text{if } x > a \text{ and } x - a \ll 1. \quad (73)$$

and

$$f_\delta(x) \approx K_\delta(x - \alpha)^{\Lambda_\delta} \quad \text{if } x > \alpha \text{ and } x - \alpha \ll 1. \quad (74)$$

Then,

$$P(\text{particles crosses the filter}) \approx P(a \leq d \leq \alpha) \quad \text{if } a < \alpha, \quad (75)$$

and

$$P(\text{particles crosses the filter}) \approx K_d(P(\delta > a))^n \left[ \frac{P(\delta > a)(\Lambda_\delta + 1)}{nK_\delta} \right]^{\frac{\Lambda_d + 1}{\Lambda_\delta + 1}} \int_0^\infty e^{-s^{\Lambda_\delta + 1}} s^{\Lambda_d} ds \quad \text{if } a \geq \alpha. \quad (76)$$

Note that, if  $f_d(a^+) = \lim_{x \rightarrow a^+} f_d(x) \neq 0$ , then  $K_d = f_d(a^+)$  and  $\Lambda_d = 0$ . Analogously, if  $f_\delta(a^+) = \lim_{x \rightarrow a^+} f_\delta(x) \neq 0$ , then  $K_\delta = f_\delta(a^+)$  and  $\Lambda_\delta = 0$ .

*Proof.* The formula in equation (75) is the asymptotic limit for  $n$  large of equation (68). We first note that, if  $a < \alpha$  then

$$\int_0^{+\infty} (P(\delta > x))^n f_d(x) dx = \int_a^\alpha (P(\delta > x))^n f_d(x) dx + \int_\alpha^{+\infty} (P(\delta > x))^n f_d(x) dx, \quad (77)$$

where the first integral equals  $P(a \leq d \leq \alpha)$  and the second integral tends to zero as  $n$  tends to infinity.

Assume now that  $a \geq \alpha$ . Note that

$$\int_0^{+\infty} (P(\delta > x))^n f_d(x) dx = \int_a^{+\infty} (P(\delta > x))^n f_d(x) dx. \quad (78)$$

Following standard asymptotic arguments we have that, for any small  $\varepsilon$ ,

$$\int_a^{+\infty} (P(\delta > x))^n f_d(x) dx \approx \int_a^{a+\varepsilon} (P(\delta > x))^n f_d(x) dx. \quad (79)$$

On the other hand, we have that

$$P(\delta > x) \approx P(\delta > a) - \frac{K_\delta(x-a)^{\Lambda_\delta+1}}{\Lambda_\delta+1} \quad \text{for } x > a \text{ and } x-a \ll 1. \quad (80)$$

Thus, we have

$$(P(\delta > x))^n \approx (P(\delta > a))^n e^{-\frac{nK_\delta(x-a)^{\Lambda_\delta+1}}{(\Lambda_\delta+1)P(\delta>a)}} \quad \text{for } x > a \text{ and } x-a \ll 1. \quad (81)$$

Plugging this expression into equation (79) and the expression (73) we get

$$\begin{aligned} \int_a^{+\infty} (P(\delta > x))^n f_d(x) dx &\approx K_d(P(\delta > a))^n \int_a^{a+\varepsilon} (x-a)^{\Lambda_d} e^{-\frac{nK_\delta(x-a)^{\Lambda_\delta+1}}{(\Lambda_\delta+1)P(\delta>a)}} dx \\ &\approx K_d(P(\delta > a))^n \int_a^\infty (x-a)^{\Lambda_d} e^{-\frac{nK_\delta(x-a)^{\Lambda_\delta+1}}{(\Lambda_\delta+1)P(\delta>a)}} dx, \end{aligned} \quad (82)$$

from where the validity of the observation follows.  $\square$

#### 4.2.1.2 Examples

We now evaluate the formula in equation (75) for several classical random distributions.

We recall that a random variable  $X$  has a uniform distribution between  $a$  and  $b$  if its probability distribution function  $f$  satisfies

$$f(x) = \begin{cases} 1/(b-a) & \text{for } a < x < b \\ 0 & \text{elsewhere.} \end{cases} \quad (83)$$

Uniform distribution variables between  $a$  and  $b$  are denoted by  $X \sim U(a, b)$ .

A random variable  $X$  has a triangular distribution between  $a$  and  $b$  with mode  $c$  if

$$f(x) = \begin{cases} 2(x-a)/[(b-a)(c-a)] & a \leq x \leq c \\ 2(b-x)/[(b-a)(b-c)] & c < x \leq b \\ 0 & \text{elsewhere.} \end{cases} \quad (84)$$

**Table 1:** Asymptotic value in the  $n$  large limit of the probability  $P$  that a particle of diameter with distribution  $d$  crosses through a one-dimensional tube of  $n$  channels of width with distribution  $\delta$  without being trapped. The probabilities in the last column are calculated according to equation (75).

$d$	$\delta$	$K_d$	$\Lambda_d$	$K_\delta$	$\Lambda_\delta$	$P$
$U(0.2, 0.6)$	$U(0.1, 0.5)$	2.5	0	2.5	0	$(3/4)^{n+1} (1/n)$
$U(0.2, 0.6)$	$U(0.2, 0.7)$	2.5	0	2	0	$(1/n) 1.25$
$U(0.2, 0.6)$	$\text{tri}(0.2, 0.6, 0.4)$	2.5	0	25	1	$(1/n)^{1/2} 0.63$
$U(0.6, 1.0)$	$\text{tri}(0.6, 1.0, 0.8)$	2.5	0	25	1	$(1/n)^{1/2} 0.63$
$U(0, 1)$	$\Gamma(3, 0.2)$	1	0	125	2	$(1/n)^{1/3} 0.26$
$\text{tri}(0.2, 0.6, 0.4)$	$U(0.2, 0.6)$	25	1	2.5	0	$(1/n)^2 4$

Triangular distribution variables are denoted by  $X \sim \text{tri}(a, b, c)$ .

A random variable  $X$  has a gamma distribution with scale  $\theta$  and shape  $\kappa$ , where  $\Gamma(\kappa)$  is the well known  $\Gamma$  function if

$$f(x) = \begin{cases} x^{\kappa-1} e^{-x/\theta} \theta^{-\kappa} / \Gamma(\kappa) & x > 0 \\ 0 & \text{elsewhere.} \end{cases} \quad (85)$$

Gamma distribution variables are denoted by  $X \sim \Gamma(\kappa, \theta)$ .

In table 1 we evaluate the formula in equation (75) with different probability distributions for the width of the channels  $\delta$  and the diameter of the particles  $d$ .

In the first example, the probability of a channel being thinner than the minimum possible particle diameter  $a$  is strictly positive. In this case, the probability of crossing without being trapped goes to zero exponentially. In the rest of the cases, the minimum possible channel width  $\alpha$  and the minimum possible particle diameter  $a$  are equal,  $\alpha = a$ . Thus, the probability of crossing without being trapped decreases as a power of  $1/n$ , which converges slower.

#### 4.2.2 Two dimensional filters

In this subsection we compute the probability that a particle flows through a two-dimensional clean filter without being trapped. We focus on the dependence of this

**Table 2:** Numerically computed values of the probability  $P$  that a particle flows through the clean filter without being trapped. Figure 24 shows the associated linear fit for the logarithms.

Square network $d \sim U(0.2, 0.5)$ $\delta \sim U(0.2, 0.5)$		
$n$	network	1-D
20	0.0854	0.0500
40	0.0488	0.0250
80	0.0277	0.0125
160	0.0143	0.0063
320	0.0067	0.0031
640	0.0044	0.0016
network fit $P = 1.06 n^{-0.84}$		one-dimensional $P = n^{-1}$

probability on the height of the filter that we denote by  $n$ . The studies in this subsection are the results of numerical simulations. We consider two different regular geometries: 1) square networks, where all the sides have the same length and are either parallel or perpendicular to the top and bottom boundaries and 2) hexagonal networks, where some of the edges are perpendicular to the top and bottom boundaries and all the edges of the hexagon have the same length.

In square networks, the height  $n$  is the distance between the top and bottom boundaries divided by the length of an edge. In hexagonal networks, the height  $n$  is the number of edges that has the shortest path between the bottom and the top boundaries.

The results of our simulations are summarized in the tables 2, 3, 4 and 5 and the figures 24, 25, 26 and 27. Note that we have compared our computations on networks with the asymptotics of the corresponding one-dimensional problem described in the previous subsection. We have also fitted the computed probabilities to functions of the form  $b/n^\beta$  and have compared these fits to the asymptotics for the one-dimensional problem given by equation (75). Our plots are in  $\log_2 - \log_2$  scale.

In a square network a particle has more possible paths to follow than in a one

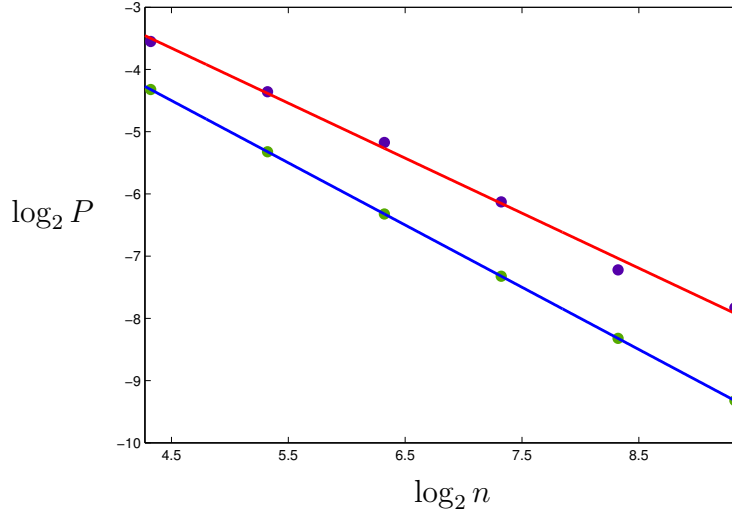


**Figure 24:** Linear fits for values from table 2 in  $\log_2 - \log_2$  scale. The purple dots are the numerically computed  $P$  probabilities. The red line is the linear fit for these points. The green dots are the one-dimensional asymptotics, and the blue line its linear fit.

**Table 3:** Numerically computed values of the probability  $P$  that a particle flows through the clean filter without being trapped. Note that tables (a) and (b) have equal one-dimensional fit. Figure 25 shows the associated linear fits for the logarithms.

hexagonal network $d \sim U(0.2, 0.5)$ $\delta \sim U(0.2, 0.5)$		
$n$	network	1-D
20	0.0839	0.0500
40	0.0431	0.0250
80	0.0261	0.0125
160	0.0120	0.0063
320	0.0073	0.0031
640	0.0036	0.0016
network fit $P = 1.23n^{-0.90}$		one-dimensional $P = n^{-1}$

(a)

hexagonal network $d \sim U(0.45, 0.5)$ $\delta \sim U(0.45, 0.5)$		
$n$	network	1-D
20	0.0533	0.0500
40	0.0262	0.0250
80	0.0142	0.0125
160	0.0060	0.0063
320	0.0039	0.0031
640	0.0016	0.0016
network fit $P = 1.05n^{-0.99}$		one-dimensional $P = n^{-1}$

(b)

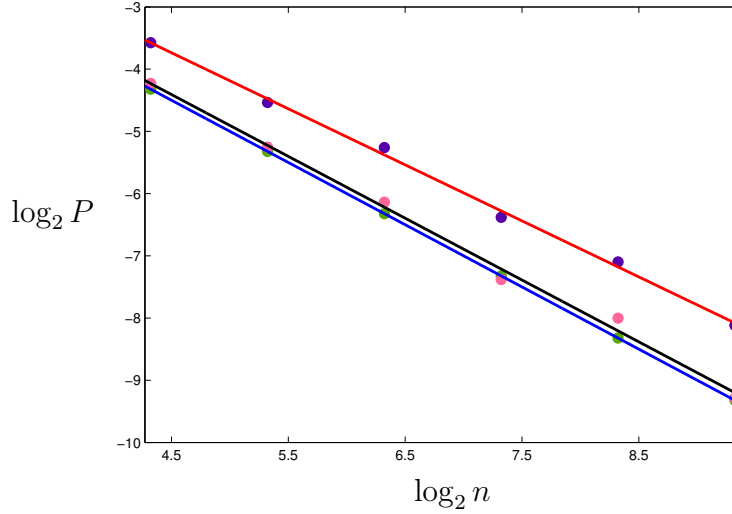


**Figure 25:** Linear fits for values from tables 3 in  $\log_2 - \log_2$  scale. The purple dots are the numerically computed  $P$  probabilities of table 3(a). The red line is the linear fit for these points. The pink dots and black line corresponds to 3(b). The green dots are the one-dimensional asymptotics, and the blue line its linear fit. Recall that one-dimensional asymptotics is equal for both networks.

**Table 4:** Numerically computed values of the probability  $P$  that a particle flows through the clean filter without being trapped. Note that tables (a) and (b) have equal one-dimensional fit. Figure 26 shows the associated linear fits for the logarithms.

Square network $d \sim U(0.2, 0.6)$ $\delta \sim \text{tri}(0.2, 0.6, 0.4)$		
$n$	network	1-D
20	0.1883	0.1409
40	0.1367	0.0996
80	0.1053	0.0704
160	0.0748	0.0498
320	0.0551	0.0352
640	0.0348	0.0249
network fit $P = 0.73n^{-0.45}$		one-dimensional $P = 0.63n^{-0.50}$

(a)

Square network $d \sim U(0.6, 1.0)$ $\delta \sim \text{tri}(0.6, 1.0, 0.8)$		
$n$	network	1-D
20	0.1583	0.1409
40	0.1164	0.0996
80	0.0820	0.0704
160	0.0575	0.0498
320	0.0415	0.0352
640	0.0322	0.0249
network fit $P = 0.66n^{-0.48}$		one-dimensional $P = 0.63n^{-0.50}$

(b)

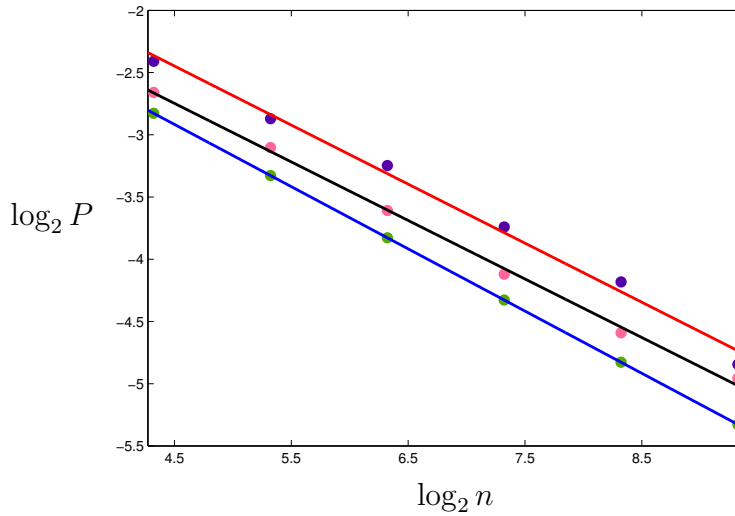


**Figure 26:** Linear fits for values from tables 4 in  $\log_2 - \log_2$  scale. The purple dots are the numerically computed  $P$  probabilities of table 4(a). The red line is the linear fit for these points. The pink dots and black line corresponds to 4(b). The green dots are the one-dimensional asymptotics, and the blue line its linear fit. Recall that one-dimensional asymptotics is equal for both networks.

**Table 5:** Numerically computed values of the probability  $P$  that a particle flows through the clean filter without being trapped. Figure 27 shows the associated linear fit for the logarithms.

Square network $d \sim U(0, 1)$ $\delta \sim \Gamma(3, 0.2)$		
$n$	network	1-D
20	0.2706	0.0942
40	0.2344	0.0754
80	0.2105	0.0601
160	0.1863	0.0478
320	0.1615	0.0380
640	0.1462	0.0302
network fit $P = 0.46n^{-0.18}$		one-dimensional $P = 0.26n^{-0.33}$

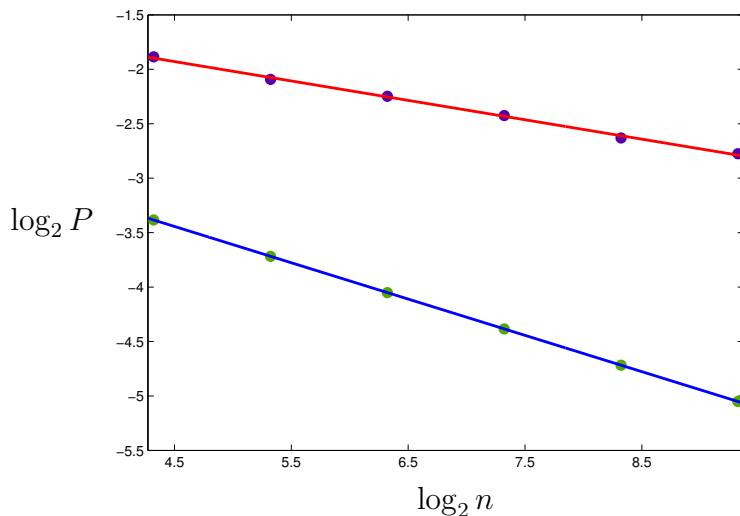


**Figure 27:** Linear fits for values from table 5 in  $\log_2 - \log_2$  scale. The purple dots are the numerically computed  $P$  probabilities. The red line is the linear fit for these points. The green dots are the one-dimensional asymptotics, and the blue line its linear fit.

dimensional network. Moreover, the flow rate is generally larger along paths with wider channels and thus, particles in a square network are more likely to travel along path with relatively wide channels. Thus, it is expected, and confirmed in our tables and graphs, that the probability that a particle crosses the square network is larger than the probability that a particle crosses a one dimensional network of the same height and with the same probability distributions for the channel widths and particle diameters.

A second observation that we draw from our calculations is that the probability that a particle crosses the square network has an asymptotic of the same class as the probability that a particle crosses a one dimensional network, i.e. of the form  $b/n^\beta$ . While the coefficient  $b$  differs from the one corresponding to the one-dimensional case, the exponent  $\beta$  seems, at least in some cases, to be equal to the one corresponding to the one-dimensional case.

In the comparisons between networks with equal asymptotics for the one-dimensional case, we observe that two-dimensional networks with smaller relative variance in the

channel thickness distribution  $\delta$  (see table 3(b) and table 4(b)) behaves closer to the one-dimensional case than networks with a bigger relative variance (see table 3(a) and table 4(a)). Thus, we identify the relative variance of the distribution  $\delta$  as an important factor differentiating one and two dimensional filters.

### 4.3 *Numerical simulations of filters*

In this section we consider our full problem. Particles enter the filter through the bottom boundary. Some exit the filter through the top boundary and others are trapped according to the laws described in section 4.1. We study the evolutions of different filters, i.e. different geometries and different probability distributions for the channels width and particles diameters. We apply the same pressure difference between top and bottom boundary to all our filters. The filter is considered useless, in which case the numerical simulation is stopped, when either one of the following occurs:

- The average flow rate drops below a certain critical value  $\alpha$ ,
- The proportion of particles crossing the filter without begin trapped becomes larger than another critical value  $\beta$ .

Note that the average flow rate is calculated after every condition change during the simulation, i.e. every time a particle is trapped or detached.

Initially, all the channels are open. At this initial stage, the pressures at the nodes and velocities within the channels are calculated using an  $LDL^T$  decomposition of the corresponding system of equations. The matrix associated with this system is banded with bandwidth of approximately the minimum between rows and columns and thus, this  $LDL^T$  can be computed in the order of the square of the number of nodes or less. Note that every time a channel is clogged or opened, the linear system has to be solved again. Fortunately, the  $LDL^T$  decomposition can be updated relatively fast.

**Table 6:** Results from numerical simulations. We compare the cleaned fluid (per column of the network), the percentage of clogged channels and the average life flow rate (per column of the network) for different filters.

<i>Network</i>	$\delta$	Cleaned	Clogged	life avg flow rate
squares	$U(0.2, 0.5)$	81.5	1.3	$0.24 * 10^{-5}$
squares	$U(0.18, 0.5)$	186.2	2.6	$0.09 * 10^{-5}$
squares	$\text{tri}(0.1, 0.5, 0.3)$	139.4	2.0	$0.30 * 10^{-5}$
squares	discrete $p = 0.35$	212.8	3.2	$0.20 * 10^{-5}$
squares	discrete $p = 0.5$	1222.1	16.5	$0.22 * 10^{-5}$
squares	discrete $p = 0.55$	1304.4	17.7	$0.50 * 10^{-5}$
squares	discrete $p = 0.6$	1016.6	13.8	$0.78 * 10^{-5}$
squares	class $\mathcal{A}$	3713.6	50.5	$1.41 * 10^{-5}$

As a consequence, the initial system is solved in the order of the square of the number of nodes or less and every subsequent system (i.e. every new system after a particle is trapped or detached) is solved in the order of the of the number of nodes to the  $3/2$  power.

Our results are summarized in table 6. Each result in that table is the average of 100 realizations. All the filters considered are square networks with 40 channels height and 200 channels width. In all our filters we assume that the volume fractions of particles in the suspension is 0.001 and the particle diameter distribution  $d$  is uniform between 0.2 and 0.5. Thus, the filters are differentiated by the probability distribution of the width of the channels, i.e. the random variable  $\delta$ . The filters considered have the following probability distribution for  $\delta$ : 1)  $U(0.2, 0.5)$ ; 2)  $U(0.18, 0.5)$ ; 3)  $\text{tri}(0.1, 0.5, 0.3)$ ; 4)  $P(\delta = 0.5) = 0.35$  and  $P(\delta = 0.2) = 0.65$ ; 5)  $P(\delta = 0.5) = 0.5$  and  $P(\delta = 0.2) = 0.5$ ; 6)  $P(\delta = 0.5) = 0.55$  and  $P(\delta = 0.2) = 0.45$ ; and 7)  $P(\delta = 0.5) = 0.6$  and  $P(\delta = 0.2) = 0.4$ . In addition, we have considered a deterministic filter. This is a filter of class  $\mathcal{A}$ , as defined in chapter 2. The thin channels have width 0.2 and the thick channels have width 0.5 and are selected as explained in chapter 2 and shown in the square network of figure 12.

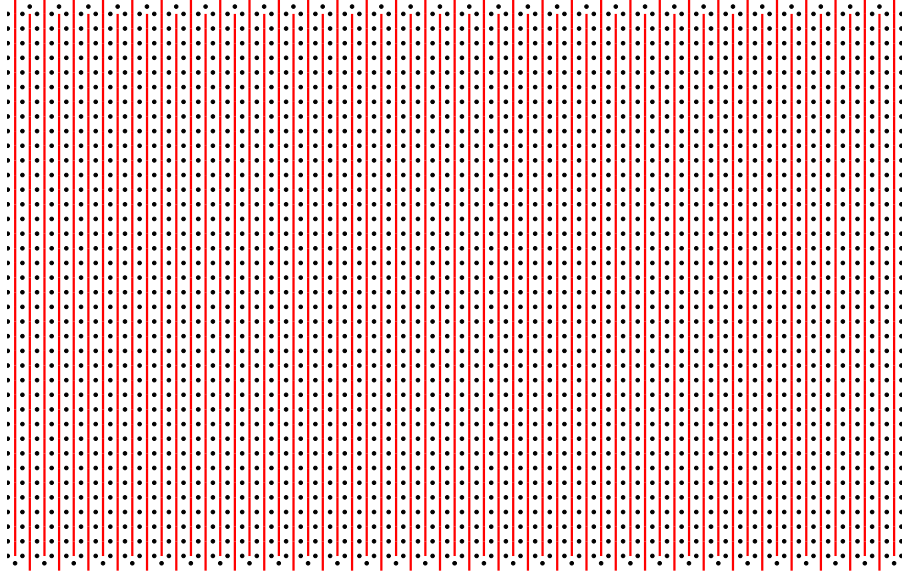


**Figure 28:** A section of a square filter of class  $\mathcal{A}$  after clogging. The clogged channels are not shown, and a trapped particle is shown instead. The thick channels are in red. All the thin channels are clogged.

A few observations can be made from the results displayed in table 6. As expected from the discussions of chapter 2, the filter of class  $\mathcal{A}$  performs the best. It traps the largest number of particles. The life average flow rate (i.e. the average flow rate over the life of the filter) is the largest. No particle flows through the filter without being trapped. See figure 28.

The life of the filters with  $U(0.2, 0.5)$  distribution for the width of the channels is short. After a relatively low number of channels clog, most of them near the bottom boundary, the probability that a particle crosses the filter exceeds the critical value  $\beta$  (that we chose to be  $\beta = 0.05$ ) and the filter is no longer useful. Note that, from the analysis of section 4.2, we expect that the probability that a particle crosses the filter without being trapped to be of the order of  $1/n$ , where  $n = 40$  in our examples.

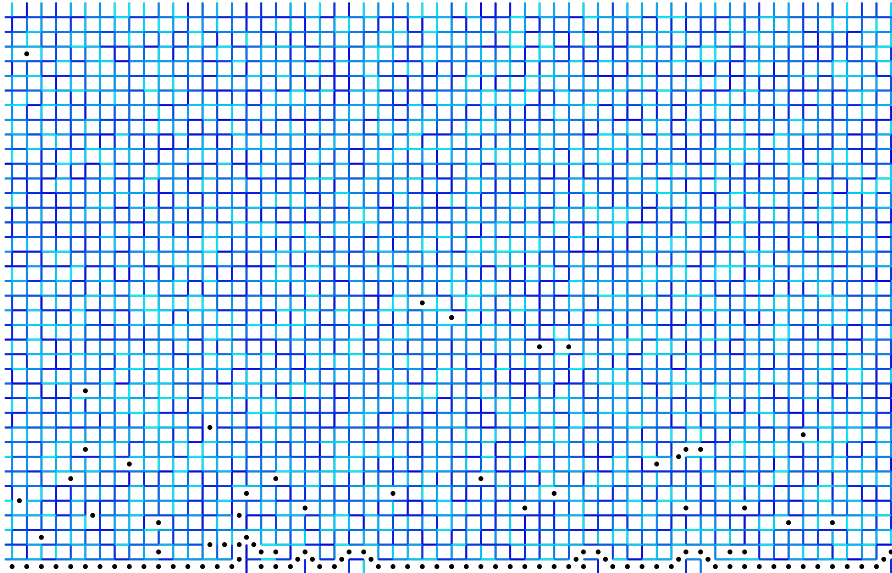


**Figure 29:** A section of a filter with  $\delta \sim U(0.18, 0.5)$  after clogging. The clogged channels are not shown, and a trapped particle is shown instead. The color intensity of the open channels indicates width, varying from blue, that corresponds to 0.5 to light blue, that corresponds to 0.18. Note that most particles are trapped close to the bottom boundary.

The analysis of that section also suggests a fix to that problem. More precisely, this deficiency is partially resolved by changing the distribution for the width of the channels to  $U(0.18, 0.5)$ . We now expect the probability that a particle crosses the filter without being trapped to be of the order of  $n^{-1}((0.5 - 0.2)/(0.5 - 0.18))^n$ . In fact, we see from our table that this filter has a longer life. Nevertheless, this is not a complete fix because most channels near the bottom boundary will clog fast and thus, the average flow rate will decrease relatively fast making the filter useless. This is illustrated in figure 29.

Regarding the filters with discrete probability distribution of the width of the channels, i.e.  $P(\delta = 0.5) = p$  and  $P(\delta = 0.2) = (1 - p)$  we observe the following.

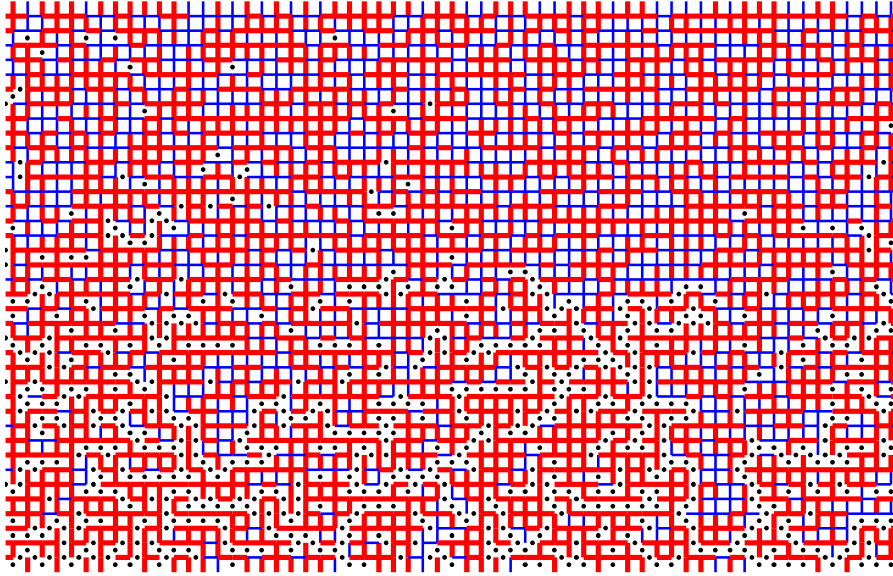


**Figure 30:** A section of a filter with discrete probability distribution  $P(\delta = 0.5) = 0.55$  after clogging. The thick channels are in red, the thin open channels in blue, and there is a particle whenever a channel is clogged. We note that the percolating paths of thick channels are few.

When  $p$  is small (smaller than  $1/2$  in the  $n \rightarrow \infty$  limit), there are no percolating paths of thick channels and thus, the filter traps all the particles and ceases its life when the flow rate decreases to the critical value  $\alpha$ . On the other hand, when  $p$  is large (larger than  $1/2$  in the  $n \rightarrow \infty$  limit), there are percolating paths of thick channels and thus, after some thin channels clog, the particles start crossing the filter at a large enough rate that the filter is no longer useful. The optimal value of  $p$  of those we explored in table 6 is  $p = 0.55$ . See figure 30.

## APPENDIX A

### ***A.1 Calculation of $\sigma$ as a function of $u$***

From equation (32), using the inverse function theorem and simple manipulations, we obtain

$$\frac{du}{dr} = -\frac{u^2}{A} (1 - e^{-\frac{\alpha}{u}})^{-1} \quad (86)$$

On the other hand, multiplying equation (32) by  $Au/\alpha$  we get

$$ru = A - A\frac{u}{\alpha} (1 - e^{-\frac{\alpha}{u}}). \quad (87)$$

Taking derivative with respect to  $r$  in the above equation and using equations (86) and (87) after some manipulation we obtain that

$$\sigma = \frac{1}{r} \frac{d(ru)}{dr} = \frac{u^2}{A} \left[ 1 - \left( 1 + \frac{\alpha}{u} \right) e^{-\frac{\alpha}{u}} \right] (1 - e^{-\frac{\alpha}{u}})^{-1} \left[ \frac{\alpha}{u} - (1 - e^{-\frac{\alpha}{u}}) \right]^{-1}. \quad (88)$$

Note that, for all  $s > 0$ ,  $1 + s < e^s$ . This implies that the factor  $1 - (1 + \alpha/u)e^{-\alpha/u}$  in the right hand side of the above equation is positive. It is easy to show that the other factors are also positive. Thus,  $\sigma(r)$  is positive for all  $r$ .

### ***A.2 $\sigma$ is an increasing function of $u$***

It is relatively easy to show that the following functions are increasing functions of  $u$ :

$$f_1(u) = \frac{u^2}{A} \left[ 1 - \left( 1 + \frac{\alpha}{u} \right) e^{-\frac{\alpha}{u}} \right], \quad (89)$$

$$f_2(u) = (1 - e^{-\frac{\alpha}{u}})^{-1}, \quad (90)$$

and

$$f_3(u) = \left[ \frac{\alpha}{u} - (1 - e^{-\frac{\alpha}{u}}) \right]^{-1}. \quad (91)$$

More precisely, taking derivatives and some simple algebraic manipulations, we have

$$f_1'(u) = \frac{2u}{A} \left[ 1 - \left( 1 + \frac{\alpha}{u} + \frac{\alpha^2}{2u^2} \right) e^{-\frac{\alpha}{u}} \right], \quad (92)$$

$$f_2'(u) = \frac{\alpha}{u^2} e^{-\frac{\alpha}{u}} (1 - e^{-\frac{\alpha}{u}})^{-2}, \quad (93)$$

and

$$f_3'(u) = \frac{\alpha}{u^2} (1 - e^{-\frac{\alpha}{u}}) \left[ \frac{\alpha}{u} - (1 - e^{-\frac{\alpha}{u}}) \right]^{-2}. \quad (94)$$

It is immediate that  $f_2'(u)$  and  $f_3'(u)$  are positive for  $u > 0$ . Noting that  $1 + \alpha/u + \alpha^2/(2u^2) < e^{\alpha/u}$  for  $u > 0$ , it also follows that  $f_1'(u)$  is positive for  $u > 0$ . Since  $\sigma(u) = f_1(u)f_2(u)f_3(u)$ , we conclude that  $\sigma$  is an increasing function of  $u$ .

### ***A.3 $\sigma$ is a decreasing function of $r$***

From the last subsection we know that  $\sigma$  is an increasing function of  $u$ . From the observations in the subsection 3.2.4, we also know that  $u$  is a decreasing function of  $r$ . Thus, we conclude that  $\sigma$  is a decreasing function of  $r$ .

### ***A.4 Calculation $d\bar{z}/d\bar{u}$ used in section 3.5.3***

The variables  $\bar{z}$ ,  $\bar{r}$  and  $\bar{u}$  are defined in the subsection 3.5.3. Applying the implicit function theorem, we have

$$\frac{d\bar{z}}{d\bar{u}} = \frac{d\bar{z}}{dt} \left( \frac{d\bar{r}}{dt} \right)^{-1} \left( \frac{d\bar{u}}{d\bar{r}} \right)^{-1}. \quad (95)$$

The different derivatives in the above equation result from equations (39) and (86)

$$\frac{d\bar{z}}{dt} = \sigma \bar{z}, \quad (96)$$

$$\frac{d\bar{r}}{dt} = -\bar{u} \quad (97)$$

and

$$\frac{d\bar{u}}{d\bar{r}} = -\frac{u^2}{A} (1 - e^{-\frac{\alpha}{u}})^{-1}. \quad (98)$$

Using the expression for  $\sigma$  as a function of  $u$  given by equation (88) we obtain the equation (43).

### A.5 Asymptotic form of the curve in figure 19

The curve in figure 19 are the pairs of parameters  $(z_*/z_0, A/(\alpha R_\ell))$  for which there exists  $s_c$  such that

$$\frac{A}{\alpha R_\ell} = \frac{s_c}{1 - s_c \left(1 - e^{-\frac{1}{s_c}}\right)}. \quad (99)$$

and

$$\frac{z_*}{z_0} = \frac{1}{1 - s_c \left(1 - e^{-\frac{1}{s_c}}\right)}. \quad (100)$$

Relatively straight forward calculations show that

$$\frac{z_*}{z_0} - 1 \approx s_c \quad \text{and} \quad \frac{A}{\alpha R_\ell} \approx s_c \quad \text{for } s_c \ll 1, \quad (101)$$

and

$$\frac{z_*}{z_0} \approx 2s_c \quad \text{and} \quad \frac{A}{\alpha R_\ell} \approx 2s_c^2 \quad \text{for } s_c \gg 1, \quad (102)$$

from where the validity of the observation 3.5.5 follows.

### A.6 Calculation $d\bar{t}/d\bar{u}$ used in section 3.5.6

The variables  $\bar{z}$ ,  $\bar{r}$  and  $\bar{u}$  are defined in the subsection 3.5.3. Applying the implicit function theorem, we have

$$\frac{d\bar{t}}{d\bar{u}} = \left(\frac{d\bar{r}}{d\bar{t}}\right)^{-1} \left(\frac{d\bar{u}}{d\bar{r}}\right)^{-1}. \quad (103)$$

Equation (55) follows from the above equation and equations (97) and (98).

### A.7 Asymptotic form of clogging time $t_c$ for large flow rates

We study the parameter regime  $A/(\alpha R_\ell) \gg 1$ . From equation (53) and some manipulation we obtain that

$$\frac{u_\ell}{\alpha} \approx \sqrt{\frac{A}{2\alpha R_\ell}}. \quad (104)$$

Then, from equation (54) and some manipulation we obtain that

$$\frac{u_0}{\alpha} \approx \frac{z_0}{z_*} \sqrt{\frac{A}{2\alpha R_\ell}}. \quad (105)$$

Plugging the last two expressions in equation (56) and some manipulation leads to equation (57).

## REFERENCES

- [1] BAI, R. B. and TIEN, C., “Effect of deposition in deep-bed filtration: Determination and search of rate parameters,” *Journal of Colloid and Interface Science*, vol. 231, no. 2, pp. 299–311, 2000.
- [2] BATCHELOR, G. K., *An Introduction to Fluid Dynamics*. Cambridge: Cambridge Mathematical Library, 2000.
- [3] BIGNO, Y., OYENEYIN, M. B., and PEDEN, J. M., “Investigation of pore-blocking mechanism in gravel packs in the management and control of fines migration,” *Proceedings, SPE Int. Symp. for Damage Control, Society of Petroleum Engineers*, pp. 29–40, 1994.
- [4] BOUHROUM, A. and CIVAN, F., “Study of particulates migration in gravel pack,” *Proceedings, SPE Int. Symp. for Damage Control, Society of Petroleum Engineers*, pp. 75–91, 1994.
- [5] BRYANT, S. L., MELLOR, D. W., and CADE, C. A., “Physically representative network models of transport in porous media,” *AIChE Journal*, vol. 39, no. 3, pp. 387–396, 1993.
- [6] BURGANOS, V. N., PARASKEVA, C. A., and PAYATAKES, A. C., “Three-dimensional trajectory analysis and network simulation of deep bed filtration,” *Journal of Colloid and Interface Science*, vol. 148, no. 1, pp. 167–181, 1992.
- [7] CHAN, H. C., CHEN, S. C., and CHANG, Y. I., “Simulation: the deposition behavior of brownian particles in porous media by using the triangular network

- model,” *Separation and Purification Technology*, vol. 44, no. 2, pp. 103–114, 2005.
- [8] CIVAN, F., *Reservoir Formation Damage*. Houston: Gulf Publishing, 2000.
- [9] DAGAN, G., *Flow and Transport in Porous Formations*. Berlin: Springer-Verlag, 1989.
- [10] DATTA, S. and REDNER, S., “Gradient clogging in depth filtration,” *Physical Review E*, vol. 58, no. 2, pp. 1203–1206, 1998.
- [11] DIESTEL, R., *Graph Theory*. Berlin: Springer, 2005.
- [12] DONALDSON, E. C., BAKER, A. B., and CARROL, H. B., “Particle transport in sandstones,” *SPE 6905*, 1977.
- [13] DULLIEN, F. A. L., *Porous Media. Fluid Transport and Pore Structure*. New York: Academic Press, 1992.
- [14] DUPONT, T. F. and LIU, Y., “Back and forth error compensation and correction methods for removing errors induced by uneven gradients of the level set function,” *Journal of Computational Physics*, vol. 190, no. 1, pp. 311–324, 2003.
- [15] FATT, I., “The network model of porous media-i. capillary pressure characteristics,” *Trans. AIME*, vol. 207, pp. 144–159, 1956.
- [16] FATT, I., “The network model of porous media-ii. dynamic properties of a single size tube network,” *Trans. AIME*, vol. 207, pp. 160–163, 1956.
- [17] FATT, I., “The network model of porous media-iii. dynamic properties of networks with tube radius distribution,” *Trans. AIME*, vol. 207, pp. 164–181, 1956.
- [18] FEDERICO, F. and MUSSO, A., “Some advances in the geometric-probabilistic method for filter design,” in *Filter in geotechnical and hydraulic engineering*

- (BRAUNS, J., SCHULER, U., and HEIBAUM, M., eds.), pp. 75–82, Rotterdam: Balkema, 1993.
- [19] GRIMMET, G., *Percolation. Second edition.* Berlin: Springer, 1999.
- [20] GRUESBECK, C. and COLLINS, E., “Entrainment and deposition of fine particles in porous media,” *Society of Petroleum Engineers Journal*, pp. 847–856, 1982.
- [21] HAMPTON, J. H. D., SAVAGE, S. B., and DREW, R. A. L., “Computer modelling of filter pressing and clogging in a random tube network,” *Chemical Engineering Science*, vol. 48, no. 9, pp. 1601–1611, 1993.
- [22] HERZIG, J. P., LECLERC, D. M., and GOFF, P. L., “Flow of suspensions through porous media - application to deep filtration,” *Industrial and Engineering Chemistry*, vol. 62, no. 5, pp. 8–35, 1970.
- [23] IMDAKM, A. O. and SAHIMI, M., “Transport of large particles in flow through porous media,” *Phys. Rev. A*, vol. 36, no. 11, pp. 5304–5309, 1987.
- [24] IMDAKM, A. O. and SAHIMI, M., “Computer-simulation of particle-transport processes in flow through porous media,” *Chemical engineering science*, vol. 46, no. 8, pp. 1977–1993, 1991.
- [25] INDRARATNA, B. and LOCKE, M. R., “Design methods for granular filters - critical review,” *Proceedings of the institution of civil engineers-geotechnical engineering*, vol. 137, no. 3, pp. 137–147, 1999.
- [26] ISON, C. R. and IVES, K. J., “Removal mechanisms in deep bed filtration,” *Chemical Engineering Science*, vol. 24, pp. 717–729, 1969.
- [27] JAMES M. MONTGOMERY, CONSULTING ENGINEERS, I., *Water treatment principles and design.* New York: John Wiley & Sons, 1985.

- [28] JOHNSON, P. R., SUNG, N., and ELIMELECH, M., “Colloid transport in geochemically heterogeneous porous media: Modeling and measurements,” *Environ. Sci. Technol.*, vol. 30, pp. 3284–3293, 1996.
- [29] JOHNSTON, P. R., *A Survey of Test Methods in Fluid Filtration*. Houston: Gulf Publishing, 1995.
- [30] KENNEY, T. C., CHAHAL, R., CHIU, E., OFOEGBU, G. I., OMANGE, G., and UME, C., “Controlling constriction sizes of granular filters,” *Canadian Geotechnical Journal*, vol. 22, pp. 32–43, 1985.
- [31] KHILAR, K. C. and FOGLER, H. S., *Migration of Fines in Porous Media*. Dordrecht: Kluwer Academic Publishers, 1998.
- [32] KIM, Y. S. and WHITTLE, A. J., “Filtration in a porous granular medium: 2. application of bubble model to 1-d column experiments,” *Transport in porous media*, vol. 65, no. 2, pp. 309–335, 2006.
- [33] LEE, J. and KOPLIK, J., “Network model for deep bed filtration,” *Physics of Fluids*, vol. 13, no. 5, pp. 1076–1086, 2001.
- [34] LOCKE, M. R., INDRARATNA, B., and ADIKARI, G., “Time dependent particle transport through granular filters,” *Journal of geotechnical and geoenvironmental engineering*, vol. 127, no. 6, pp. 521–529, 2001.
- [35] LOGAN, B. E., *Environmental Transport Processes*. New York: John Wiley & Sons, 1999.
- [36] LOGAN, B. E., JEWETT, D. G., ARNOLD, R. G., BOUWER, E. J., and O’MELIA, C. R., “Clarification of clean-bed filtration models,” *J. Environ. Eng.*, vol. 121, no. 12, pp. 869–873, 1995.

- [37] LOGAN, J. D., *Transport Modeling in Hydrogeochemical Systems*. New York: Springer-Verlag, 2001.
- [38] MCDOWELL-BOYER, L. M., HUNT, J. R., and SITAR, N., "Particle transport through porous media," *Water Resources Research*, vol. 22, pp. 1901–1921, 1986.
- [39] MUECKE, T. W., "Formation fines and factors controlling their movement in porous media," *Journal of Petroleum Technology*, vol. 31, pp. 144–150, 1979.
- [40] OYENEYIN, M. B., PEDEN, J. M., HOSSEINI, A., and REN, R., "Factors to consider in the effective management and control of fines migration in high permeability sands," *Journal of the Society of Petroleum Engineers*, pp. 355–360, 1995.
- [41] PANDYA, V. B., BHUNIYA, S., and KHILAR, K. C., "Existence of a critical particle concentration in plugging of a packed bed," *AIChE Journal*, vol. 44, pp. 978–981, 1998.
- [42] RAJAGOPALAN, R. and TIEN, C., "Trajectory analysis of deep bed filtration using the sphere in cell porous media model," *AIChE Journal*, vol. 22, no. 3, pp. 523–533, 1976.
- [43] REGE, S. D. and FOGLER, H. S., "A network model for deep bed filtration of solid particles and emulsion drops," *AIChE Journal*, vol. 34, no. 11, pp. 1761–1772, 1988.
- [44] RYAN, J. N. and ELIMELECH, M., "Colloid mobilization and transport in groundwater," *Colloids and Surfaces A. Physicochemical and Engineering Aspects*, vol. 107, pp. 1–56, 1996.
- [45] SAHIMI, M., *Applications of Percolation Theory*. London: Taylor & Francis, 1994.

- [46] SAHIMI, M., GAVALAS, G. R., and TSOTSIS, T. T., "Statistical and continuum models of fluid-solid reactions in porous media," *Chemical Engineering Science*, vol. 45, no. 6, pp. 1443–1502, 1990.
- [47] SAIERS, J. E., HORNBERGER, G. M., and LIANG, L., "First- and second-order kinetics approaches for modeling the transport of colloidal particles in porous media," *Water Resour. Res.*, vol. 30, no. 9, pp. 2499–2506, 1994.
- [48] SAKTHIVADIVEL, R. and EINSTEIN, H. A., "Clogging of porous column of spheres by sediment," *ASCE Journal of Hydraulic Engineering*, vol. 96, pp. 461–472, 1970.
- [49] SCHEIDEGGER, A. E., *The physics of flow through porous media, 2nd edn.* Toronto: Toronto University Press, 1963.
- [50] SHARMA, M. M. and YORTSOS, Y. C., "Fines migration in porous media," *AIChE Journal*, vol. 33, pp. 1654–1662, 1987.
- [51] SHARMA, M. M. and YORTSOS, Y. C., "A network model for deep bed filtration processes," *AIChE Journal*, vol. 33, pp. 1644–1653, 1987.
- [52] SHERARD, J. L., DUNNIGAN, L. P., and TALBOT, J. R., "Basic properties of sand and gravel filters," *Journal of Geotechnical Engineering*, vol. 110, pp. 684–701, 1984.
- [53] SHERARD, J. L., DUNNIGAN, L. P., and TALBOT, J. R., "Filters for silts and clays," *Journal of Geotechnical Engineering*, vol. 110, pp. 701–718, 1984.
- [54] SILVEIRA, A., "An analysis of the problem of washing through in protective filters," *Proc. 6th Conf. Soil Mech., Montreal, Canada*, pp. 551–555, 1965.

- [55] SOO, H. and RADKE, C. J., “A filtration model for the flow of dilute, stable emulsions in porous media—i. theory,” *Chemical Engineering Science*, vol. 41, no. 2, pp. 263–272, 1986.
- [56] SUCHOMEL, B. J., CHEN, B. M., and ALLEN, M. B., “Network model of flow, transport and biofilm effects in porous media,” *Transport in Porous Media*, vol. 30, no. 1, pp. 1–23, 1998.
- [57] TERZAGHI, K., PECK, R. B., and MESRI, G., *Soil mechanics in engineering practice. Third edition*. New York: John Wiley & Sons, 1996.
- [58] THOMPSON, K. E. and FOGLER, H. S., “Modeling flow in disordered packed beds from pore-scale fluid mechanics,” *AIChE Journal*, vol. 43, no. 6, pp. 1377–1389, 1997.
- [59] TIAB, D. and DONALDSON, E. C., *Petrophysics*. Houston: Gulf Publishing, 1996.
- [60] TIEN, C. and PAYATAKES, A., “Advances in deep bed filtration,” *AIChE Journal*, vol. 25, no. 5, pp. 737–759, 1979.
- [61] VALDES, J. R., *Fines Migration and Formation Damage - Microscale Studies*. PhD thesis, Georgia Institute of Technology, 2002.
- [62] VALDES, J. R. and SANTAMARINA, J. C., “Particle clogging in radial flow: Microscale mechanism,” *SPE Journal*, vol. 11, no. 2, pp. 193–198, 2006.
- [63] WITT, K. J., “Reliability study of granular filters,” in *Filters in geotechnical and hydraulic engineering* (BRAUNS, J., SCHULER, U., and HEIBAUM, M., eds.), pp. 35–42, Rotterdam: Balkema, 1993.

- [64] YAO, K., HABIBIAN, M. T., and OMELIA, C. R., "Water and waste water filtration: concepts and applications," *Environ. Sci. Technol.*, vol. 5, no. 11, pp. 1105–1112, 1971.